Astronomy & Astrophysics manuscript no.
(will be inserted by hand later)

The new sample of Giant radio sources: I. Radio imaging, optical identification and spectroscopy of selected candidates

J. Machalski, M. Jamrozy, S. Zola

Astronomical Observatory, Jagellonian University, ul. Orla 171, PL-30244 Cracow, Poland

Received / Accepted

Abstract. A new sample of very large angular size radio sources has been selected from the 1.4 GHz VLA surveys: FIRST and NVSS. This sample will be very useful for an observational constraint on the time evolution of double radio sources, especially their size, predicted by numerous analytical models of such evolution (cf. Introduction). In this paper we present radio and optical data for a large fraction of the sample sources. They are: high-frequency VLA maps with very weak radio cores detected, deep optical images showing the identified faint host galaxies not visible on the DSS images, and optical spectra of the identified galaxies brighter than about $R \approx 18.5$ mag taken with the McDonald Observatory 2.1m telescope. For 15 galaxies (of which 4 do not belong to the complete sample) the redshift has been determined. In the result, 44 per cent of galaxies in the complete sample have redshift data (with one exception all redshifts are less than 0.33), of which 70 per cent have a linear size exceeding 1 Mpc. The photometric redshift estimates for other 11 galaxies with 19 mag$< R <$21.7 mag ($0.3 < z < 0.5$) predict their sizes much over 1 Mpc.

Key words. galaxies: active – galaxies: distances and redshift –galaxies: evolution – radio continuum: galaxies

1. Introduction

Giant double radio sources with a projected linear extent $D \geq 1$ Mpc (if $\Omega_o = 1$ and $H_o = 50$ km s^{-1}Mpc^{-1} which we use hereafter) are the largest objects in the Universe. Since the existing models of the radio source evolution (e.g. Kaiser et al. 1997; Kaiser & Alexander 1999; Blundell et al. 1999) predict that classical double sources grow in size with increasing age, these giants must represent a very late phase of the evolution of radio sources. In the analytical model of Kaiser et al. (1997), the range of luminosities and the largest linear sizes are limited mostly by the jet powers and the different processes of energy loss. The importance of adiabatic, synchrotron, and inverse Compton losses in reducing the source luminosity at large life time is so significant that the largest sources should have very low luminosity, especially at high observing frequencies. Blundell et al. argue that the samples of FRII sources are strongly affected by the effect of "youth–redshift degeneracy" causing the old sources are barely observed at high redshifts.

A natural consequence of these predictions is that the majority of giants have to be very old. On the other hand, it is not clear under what circumstances radio sources can live long enough to reach Mpc-sizes, and what fraction of their population can do that. One possibility is that the extreme sizes of some sources are related to their surrounding intergalactic medium. Mack et al. (1998), after the spectral ageing analysis of 5 giant radio galaxies, found evidence that those giants are so large because of their low-density environments and not because of higher ages. Kaiser & Alexander suggested that a few giant sources in the LRL sample (Laing et al. 1983) may "constitute a class of objects intrinsically different from the rest of the sample".

It has to be emphasized that all these studies were based on an inhomogenous collection of currently known giant sources. An ambitious project to select a uniform and large sample of giant radio sources appropriate for an extensive study of their population, has been undertaken at Leiden Observatory (e.g. Schoenmakers et al. 1998). The sample of 33 candidate sources, selected from the WENSS 325-MHz survey in the sky area of about 2.5 sr (Rengelink et al. 1997), has been studied by Schoenmakers (1999). These sources supplement a sample of 19 Giants already known in the same sky area. However, in our contribution during IAU Symposium No. 199 on the population modelling of giant FRII-type sources, we have presented evidence that only a very small fraction of expected faint giants (with 1.4 GHz flux density less than 0.5 Jy)

Send offprint requests to: J. Machalski, e-mail: : machalsk@oa.uj.edu.pl

has already been detected. In order to find the missing giant sources we have selected another sample of faint candidates for which further radio and optical observations have been done.

In this paper, the first results of (i) the radio imaging with the main effort to detect a compact radio core in those giant candidates whose cores were not detected yet, (ii) the follow-up optical identifications, and (iii) the optical spectroscopy of identified optical counterparts (with the one exception - only galaxies) are presented. In Sect. 2, the selection criteria and the list of candidates are given. The new radio observations are described in Sect. 3. The optical identification, and the deep optical imaging for those candidates whose optical counterpart is not visible on the POSS plates, are gived in Sect. 4. Finally, the optical spectroscopy of the identified galaxies bright enough that their spectrum could be taken with a medium-size telescope are presented in Sect. 5.

Basic physical parameters have been derived for the sample sources with spectroscopic redshift including their radio and optical luminosity, projected linear size, equipartition magnetic field and energy density. A photometric redshift and size estimates are provided for a few host galaxies identified in the deep optical images and for which a crude apparent R-band magnitude has been determined. These results are summarized in Sect. 6.

2. Selection criteria

We decided to select our candidates from the 1.4-GHz sky surveys: NVSS (Condon et al. 1998) and the first part of FIRST (Becker et al. 1995). These surveys, which provide radio maps made with two different angular resolutions ($45''$ and $5''$, respectively) at the same observing frequency, allowed (i) an effective removal of confusing sources, (ii) a reliable determination of its morphological type, and (iii) a determination of the compact core component necessary for the proper identification of the source with its host optical object. From the population modelling (cf. Introduction) we expected that most missing giants should be below a redshift of about 0.4. At $z \approx 0.4$, a source with a linear size of 1 Mpc will have an angular size of 2.6 arc min. Therefore, we have chosen the following selection criteria:

The radio source
(1) lies within the sky area of 0.47 sr limited by $07^{\rm h}20^{\rm m} <$ R.A.(J2000) $< 17^{\rm h}30^{\rm m}$ and $+28\overset{\circ}{.}5 <$ Decl.(J2000) $< +41\overset{\circ}{.}0$,
(2) has a morphological type (suggested from the NVSS and FIRST radio maps, Fanaroff-Riley (1974)) type II (FRII) or FRI/II,
(3) has an angular separation between the brightest regions on the maps $\Theta \gtrsim 3$ arc min, and
(4) has a 1.4 GHz flux density on the NVSS map of $S_{1.4} <$ 500 mJy.

The above criteria were fulfilled by 36 sources listed in Table 1. The entries of Table 1 are:

Column 1: IAU name at epoch J2000

Column 2: Fanaroff-Riley morphological type

Column 3: 1.4 GHz flux density from the NVSS survey

Column 4: radio spectral index around the frequency of 1.4 GHz specified as the mean of spectral indices $\alpha(325, 1400)$ and $\alpha(1400, 4850)$. If a flux density at about 5 GHz is not known, the respective spectral index is given as $> \alpha(325, 1400)$

Column 5: angular size in arc sec

Column 6: information about radio core; 'c' indicates that the core has already been detected in the FIRST survey, **'c'** – that it has been detected in this work. 'c?' indicates the lack of high-resolution map, but a compact core is very probable

Column 7: optical identification; G–galaxy, Q–quasar

Column 8: R–band apparent magnitude of the identified host object taken from the reference given in column 10. The magnitudes of faint galaxies detected in this paper (cf. Sect. 4.2 and Table 4) are marked by bold-face

Column 9: redshift of the host object (galaxy). The redshifts of 5 objects were available prior to our spectroscopical observations; the relevant references are given in column 10. Redshifts determined in this paper are marked by bold-face.

Column 10: references to optical type of the identified object and its magnitude, and to the redshift.

At the bottom of Table 1 we list 4 additional giant candidates which have been observed spectroscopically though they do not belong to the complete sample. J1218+5026, taken from the GB/GB2 sample (Machalski 1998), was supposed to be a very large source; the remaining three (J1018–1240, J1328–0307, and J1457–0613) are the largest sources among the Las Campanas radio galaxies (cf. Machalski & Condon 1999).

Notes on individual sources in Table 1:

J0816+3347: Very blue object on the DSS (E=18.76 mag; O–E= −0.04 mag). R=(20.7 ± 0.2) mag was found in March 4, 2000 (cf. Fig. 3a). A very certain variability suggests that this object may be a quasar.

J0912+3510: The source was noticed as a giant by Jamrozy & Machalski (1999) on the basis of a photometric redshift estimate derived for the brightest galaxy near the midpoint between its radio lobes (marked as galaxy A in Table 4 and in Fig. 2a). Fig. 4b shows the spectrum of galaxy A. On the other hand, the statistical effect that the radio core is predominantly closer to the brighter radio lobe (cf. Sect. 6.4) suggests another possible identification with galaxy B. Unfortunately, no radio core brighter than about 0.1 mJy beam^{-1} was detected in spite of two observational attempts (cf. Table 2).

J0927+3510: The second case where we did not detect the radio core (cf. Fig. 1a). Therefore, a probable identification is a galaxy marked as galaxy A in Table 4 and Fig. 3b. This 20.6 mag galaxy is closer to the brighter eastern lobe of the source, thus is favoured by the correlation mentioned above. The second possible identification is the 21.7 mag galaxy B lying close to the midpoint between the radio lobes (cf. Fig. 3b).

Table 1. The sample of Giant candidates

IAU name J(2000)	FR type	$S_{1.4}$ [mJy]	α	Θ [″]	radio core	opt. id.	R [mag]	z	Ref	Notes
J0720+2837	II	46	>0.7	370	c	G	17.75	**0.2705**	1,6	
J0725+3025	II	35	1.43	175	c	...	.....	.....		
J0816+3347	II	40	1.15	210	c	Q?	18.8-**20.7**	.....	1,6	+
J0912+3510	II	143	1.24	375	...	G	19.35	**0.2489**	1,6	+
						G	19.5		6	
J0927+3510	II	96	1.20	345	...	2G	**20.6**or**21.7**	.....	6	+
J1011+3111	II	70	>0.6	286	c	G	**21.2**	.....	6	
J1113+4017	I/II	246	0.74	720	c	G	14.56	0.0745	1,4	
J1155+4029	II	323	1.04	229	c	G	**21.5**	.....	6	
J1200+3449	II	223	1.05	147	**c**	G	**21.2**	.....	6	
J1253+4041	I/II	52	>0.8	275	...	G	17.27	**0.2302**	1,6	
J1254+2933	II	65	(0.6)	300	**c**	G	**20.3**	.....	6	
J1330+3850	II?	31	0.77	280	...	2G	**19.3**or**19.6**	.....	6	+
J1343+3758	II	136	0.87	678	**c**	G	17.94	**0.2267**	1,6	+
J1344+4028	I/II	222	0.78	450	c	G	14.92	**0.0748**	1,6	+
J1345+3952	II	170	1.14	167	...	G	15.80	**0.1611**	1,6	
J1355+2923	II	140	1.27	263	c	G	**20.4**	.....	6	
J1428+2918	II	431	1.10	905	c	G	13.0	0.0870	4	
J1428+3938	II	89	1.09	230	c	...	.....	.....		
J1445+3051	II	95	0.91	290	c	G	19.01	0.42	3	
J1451+3357	II	138	0.91	245	c	G	18.7	**0.3251**	6	
J1453+3309	II	460	0.96	320	c	G	18.3	0.249	4	
J1512+3050	II	98	0.67	240	c	G	15.98	**0.0895**	1,6	
J1513+3841	II?	25	>0.6	210	...	...	.....	.....		
J1525+3345	II	51	>0.8	214	c	G	**20.9**	.....	6	
J1526+3956	II	62	>1.0	536	c?	...	.....	.....		
J1554+3945	II	74	>0.8	219	**c**	G	19.5	.....	6	
J1555+3653	II	106	1.00	335	c	G	18.56	**0.2472**	1,6	+
J1604+3438	II	146	0.95	200	c?	...	.....	.....		
J1604+3731	II	122	1.05	182	c	G?	.....	0.814	2	
J1615+3826	II?	37	(0.5)	245	...	G	17.59	**0.1853**	1,6	
J1632+3433	II	29	>0.9	180	c	...	.....	.....		
J1635+3608	I/II	100	0.63	320	c	G	17.30	**0.1655**	1,6	
J1649+3114	II	153	1.10	209	c	G	19.62	.....	1	
J1651+3209	I/II	68	(0.5)	430	c	...	.....	.....		
J1712+3558	II	86	0.93	210	**c**	G	19.1	.....	6	
J1725+3923	II	88	0.95	270	c	G	18.76	.....	1	+
J1018–1240	I/II	276	1.27	555	c	G	16.36	**0.0777**	5,6	
J1218+5026	II	596	0.78	196	c?	G	17.8	**0.1995**	6	
J1328–0307	II	201	>1.2	801	c	G	16.82	**0.0860**	5,6	
J1457–0613	II	507	>1.0	235	c?	G	17.29	**0.1671**	5,6	

References: (1) the Digitized Sky Survey (DSS) data base, (2) Cotter et al. (1996), (3) Hook et al. (1998), (4) Schoenmakers (1999), (5) Machalski & Condon (1999), (6) this paper

J1330+3850: Because a radio core is unknown yet, the optical identification remains uncertain. Two possible identifications of a host galaxy are given in Table 4.

J*1343+3758:* The radio map with the core indicated is shown in Fig. 1d. A detailed analysis of this the third largest giant source known up to now is given by Machalski & Jamrozy (2000). The final corrected redshift of the identified galaxy is given in this paper.

J1344+4028: A 20 mJy background source at $13^{\rm h}44^{\rm m}46\overset{\rm s}{.}51$, $+40°26'50\overset{''}{.}6$ (J2000), contaminating the sample source, is subtracted.

J1555+3653: The sample source is slightly confused on the NVSS map by the strong steep-spectrum background source 6C155304.9+370235 (B1950).

J1725+3923: Strongly confused by two compact sources at the (J2000) positions: $17^{\rm h}25^{\rm m}18\overset{\rm s}{.}15$; $+39°21'19\overset{''}{.}0$ and $17^{\rm h}25^{\rm m}24\overset{\rm s}{.}44$; $+39°24'04\overset{''}{.}7$, hence its radio spectrum is uncertain.

3. Radio observations

Eight out of twelve sources with no radio core detected in the FIRST survey have been observed with the VLA in the B–array at 4.86 GHz and/or BnC–array at 8.46 GHz. The observing log is given in Table 2. In order to reach a *rms* noise of about 30 μJy beam^{-1} the field of view centred at a midpoint between the lobes was observed for an integration time of at least 40 min. The interferometric phases were calibrated approximately every 20 min with the phase calibrator nearest to the observed source. The source 3C286 served as the primary flux density calibrator.

The sky coordinates and the integrated flux density of the detected cores are given in Table 3. The last column of Table 3 gives the ratio of 5-GHz flux density of the core to 1.4-GHz flux density of the entire source. Unfortunately, no core brighter than about 0.1 mJy beam^{-1} was detected in the sources J0912+3510 and J0927+3510. Dividing the above limit of core flux by the total flux of these sources, one can expect their fraction $f_{\rm c}$ to be below 0.001. This is about 2 times less than that of the faintest core detected in already known giants. Also no core was detected in the source J1513+3841. In this case, the upper limit of 5 GHz flux density of the core is about 0.25 mJy beam^{-1}.

The high-frequency VLA contour maps for those sources whose extended lobes were not attenuated too much by the VLA primary beam and/or where some compact structures reside in the lobes, are presented in Figs. 1a–f. In order to show how these structures are located inside the extended emission, each contour map is overlaid onto the relevant NVSS map shown in the gray scale. The compact cores, for the sake of proper contrast, are shown by the black contours. The crosses indicate the position of the host galaxy (cf. Sect. 4).

4. Optical imaging and identification

4.1. DSS identification

To identify our source candidates whose radio core is known with a host optical object, first of all we used the 'Digitized Sky Survey' (DSS), i.e. digitized POSS survey. For 29 sample sources with cores, we have identified their cores with 13 galaxies and one very blue object, possibly a quasar. This means that the optical counterpart of one half of our giant candidates is fainter than $R \approx 20$ mag. Taking into account the R-band Hubble diagram for 3C radio galaxies (Eales 1985) and allowing the giant radio galaxies to be one magnitude less luminous than the 3C ones, $R \gtrsim 20$ mag implied a redshift $z > 0.4$. For four giant candidates without known radio core (J0912+3510, J1253+4041, J1345+3952, and J1615+3826) a very probable host galaxy has been determined. The optical fields, reproduced from the DSS and showing the presumed identification with the radio contour NVSS map overlayed, are shown in Fig. 2a–d. The R magnitudes of the identified galaxies from the DSS are listed in Table 1 with 0.01 precision.

4.2. Deep imaging

For 9 sky fields containing the sample sources, 6 of which having no radio core identification in the DSS, deep optical imaging was done with the 2.1m telescope of the McDonald Observatory (Texas). The observations were made using the 'Imaging Grism Instrument' (IGI) equipped with aTK4 1024×1024 CCD detector cooled with liquid nitrogen. IGI allows direct imaging and spectroscopy with a spatial scale of $0\overset{''}{.}48$ per pixel within the field of view of about 8×8 arc min. The sky fields centred **on** the radio source were observed through the Cousins R-band filter at zenith angles providing air masses less than 1.2, most of them being below 1.05. The exposure times applied ranged from 3 min to 10 min. Although seeing conditions during the observing night of March 4/5,2000 were not photometric ones, also the standard fields NGC 2419, NGC 4147, and M92 (Christian et al., 1985) were observed for a crude photometric calibration.

The astrometric calibration has been done by transforming the instrumental pixel coordinates of stars in the investigated frame into their sky coordinates in the DSS data base. As a result, all six sources with a core have been identified with faint galaxies. In the two remaining fields, possible galaxy identifications are found. Instrumental magnitudes of the identified host galaxies (and several other objects) on the CCD frames, reduced for bias, dark current and flat field with the ESO MIDAS package, were determined using both the aperture (MIDAS magnitude/circle procedure) and PSF (DAOPHOT II procedure; Stetson 1987) methods. These instrumental magnitudes were then transformed into R magnitudes in the twofold manner: a transformation formula was determined for (i) those objects in the particular frame whose magnitudes are calibrated in the DSS ($R_{\rm DSS}$), and (ii) standards in the calibration fields ($R_{\rm cal}$). Dispersions of the differ-

Table 2. The VLA observing log

Source	ν [GHz]	beam size [$'' \times ''$]	int. time [min]	rms noise [μJy/beam]	observing date
J0912+3510	4.86	1.3×1.0	3×11	50	May 24,1997
	8.46	3.5×0.9	2×25	21	Feb.20,2000
J0927+3510	8.46	2.8×0.9	2×26	23	Feb.20,2000
J1200+3449	8.46	2.4×0.8	2×23	44	Feb.20,2000
J1254+2933	4.86	1.3×1.2	3×23	33	Dec.13,1999
J1343+3758	4.86	1.2×1.1	3×24	30	Dec.13,1999
J1513+3841	4.86	3.0×1.1	3×22	52	Feb.12,2000
J1554+3945	4.86	3.0×1.2	3×22	43	Feb.12,2000
J1712+3558	4.86	3.2×1.1	3×22	55	Feb.12,2000

Table 3. Data of the detected radio cores

Source	ν [GHz]	R.A.(J2000)	Dec.(J2000)	$S_{\rm core}$ [mJy]	$f_{\rm c}$
J1200+3449	8.46	$12^{\rm h}00^{\rm m}50\overset{\rm s}{.}25$	$+34^\circ49'20\overset{''}{.}6$	0.36 ± 0.08	0.002
J1254+2933	4.86	12 54 34.06	+29 33 40.2	0.74 ± 0.09	0.011
J1343+3758	4.86	13 42 54.53	+37 58 18.8	1.09 ± 0.07	0.008
J1554+3945	4.86	15 54 26.92	+39 45 08.7	0.84 ± 0.09	0.011
J1712+3558	4.86	17 12 24.89	+35 58 26.2	0.55 ± 0.12	0.006

ences $\Delta R_1 = R - R_{\rm DSS}$ and $\Delta R_2 = R - R_{\rm cal}$ (the latter calculated from the calibration fields taken just before and after the target frame) have been used to determine the combined *rms* error $\Delta R = (\Delta R_1^2 + \Delta R_2^2)^{1/2}$ of particular R magnitude.

The sky coordinates, radio-minus-optical offsets with respect to the radio core, and R-magnitude estimate with its *rms* error of the identified faint galaxies are listed in Table 4. The CCD R-band frames with the deep identification marked are shown in Figs. 3a–h.

5. Optical spectroscopy

5.1. Observations

In order to determine redshifts of the identified galaxies brighter than about 18.5 mag in the R band, optical spectroscopic observations were conducted between Feb 27 and March 4, 2000. Also these observations were made with the McDonald Observatory 2.1m telescope equipped with the IGI instrument. A grism sensitive to the wavelength range of 3750 Å to 7600 Å, and a $2''$ wide slit providing a dispersion of 3.7 Å per pixel and spectral resolution of about 12 Å, were used. A number of exposures ranging from 15 min to 30 min was taken for 15 galaxies, of which only 11 belonging to the complete sample were bright enough to be observed with the 2.1m telescope. The resulting redshifts have been put in bold face in Table 1. The epoch of observations did not allow us to try to observe the identified galaxies at R.A.$> 16^{\rm h}30^{\rm m}$ (i.e. J1712+3558 and J1725+3923).

Usually two or three useable exposures were obtained for each galaxy, which made it possible to improve S/N ratio without an increase of smearing of the spectrum during a too long single exposure due to imperfect tracking of the telescope. The total integration time for each spectrum ranged from 30 min for the brightest galaxy (J1344+4028) to 90 min for the faintest ones. The wavelength calibration was carried out using exposures to helium and mercury lamps. The flux calibration was provided by exposures of a spectrophotometric standard star close to the observed galaxy, chosen from among HZ43, HZ44, EG50, EG79, GZ140, and Feige98 (Stone 1977).

5.2. Data reduction and the results

All spectra obtained were reduced in the standard way, i.e. corrected for bias, dark current and flat field, rejected cosmic rays , combined and calibrated using the LONGSLIT package of the IRAF software. One-dimensional spectra for the galaxies were extracted interactively, using the observed intensity profile along the slit to define the apertures and sky-background regions. The final 1–D spectra of the observed galaxies are shown in Figs. 4a–o. The emission lines and/or absorption bands detected, as well as the resultant redshift of these features with its *rms* error are listed in Table 5.

Most of the spectra are typical of elliptical and lenticular (E, S0) galaxies whose continuum emission with the prominent 4000 Å discontinuity is dominated by evolved giant stars (cf. Kennicutt 1992). The emission lines mostly detected are [OII]λ3727 and [OIII]λ4959 and λ5007. Also weak Balmer lines are present in some spectra, however usually only Hβ is detected because the majority of the spectra is redshifted by more than 1.1, so that in those cases the Hα line was beyond the wavelength range observed. In a few spectra the blue continuum is strong and suggests the presence of a young population of stars characteristic for early-type spirals. However these blue galaxies are too faint to be morphologically classified on

Table 4. Data of the identified faint galaxies

Source	gal.	R.A.(J2000)	Dec.(J2000)	ΔR.A. [s]	ΔDec. [″]	R±ΔR [mag]
J0912+3510	A	$09^{\rm h}12^{\rm m}51\overset{\rm s}{.}81$	$+35^\circ10'16\overset{''}{.}1$	.....	.....	19.35
	B	09 12 51.20	+35 10 07.6	.....	.....	19.5 ± 0.2
J0927+3510	A	09 27 54.93	+35 10 39.8	.....	.....	20.6 ± 0.3
	B	09 27 50.58	+35 10 50.5	.....	.....	21.7 ± 0.4
J1011+3111		10 11 12.21	+31 11 05.1	−0.07	+0.1	21.2 ± 0.3
J1155+4029		11 55 49.61	+40 29 40.8	−0.06	−0.2	21.5 ± 0.4
J1200+3449		12 00 50.56	+34 49 21.0	−0.28	−0.4	21.2 ± 0.4
J1254+2933		12 54 34.14	+29 33 41.8	−0.08	−1.6	20.3 ± 0.2
J1330+3850	A	13 30 36.33	+38 50 20.0	.....	.....	19.3 ± 0.2
	B	13 30 34.84	+38 50 19.9	.....	.....	19.6 ± 0.3
J1355+2923		13 55 17.83	+29 23 34.5	−0.18	−0.6	20.4 ± 0.2
J1525+3345		15 25 00.84	+33 45 42.9	−0.06	−1.2	20.9 ± 0.3

the digitized POSS plates. For four galaxies (J1344+4028, J1345+3952, J1512+3050, and J1635+3608) their redshift can be determined from the absorption lines CaIIλ3934 λ3968 and bands G, Mg, and Na D only.

6. Physical parameters

6.1. Determination of the parameters

The global physical parameters estimated for the sources with spectroscopic redshift are given in Table 6. The twelve columns of Table 6 give:

Column 1: IAU name of source

Column 2: Logarithm of radio luminosity at the emitted frequency of 1.4 GHz ($\log L_{1.4}$) calculated with the luminosity-distance modulus for q_o=0.5, i.e.

$$A(z) = 2(1+z) - \sqrt{1+z}$$

Column 3: Absolute R-band magnitude of the host galaxy calculated assuming it is an elliptical with an optical spectral index ($\alpha_{\rm opt}$) corresponding to the $B-R$ colour and evolving with redshift accordingly the 'c'-model of Bruzual (1983). Thus

$$M_R = R - 5\log A(z) - 2.5\{\alpha_{opt}(z) - 1\}\log(1+z) - 43.891$$

No correction for the foreground extinction has been applied because most of the galaxies have a galactic latitude $\mid b \mid > 50^\circ$.

Column 4: Logarithm of the radio–optical luminosity ratio parameter defined by

$$\log r = \log L(1.4{\rm GHz}) - \log L_{\rm opt}({\rm Rband}), {\rm where}$$

$$\log L_{\rm opt}[{\rm W\,Hz^{-1}}] = -0.4\,M_R + 13.522$$

Column 5: Linear size of source (D), i.e. projected separation between the hotspots or the brightest regions in opposite radio lobes

Column 6: Average magnetic field ($B_{\rm me}$) calculated under assumption of energy equipartition, a cylindrical geometry of the extended emission with the base diameter set equal to the average width of the lobes, usually measured half-way between the core and their brightest regions, using the prescription of Leahy & Williams (1984), a filling factor of unity, and equal distribution of kinetic energy between relativistic electrons and protons. The total radio luminosity is integrated from 10 MHz to 10 GHz.

Column 7: Minimum energy density ($u_{\rm me}$) under the same assumptions

Column 8: Ratio of the equivalent magnetic field of the microwave background radiation $B_{\rm iC} = 0.324(1+z)^2$[nT] to the equipartition magnetic field in the source $B_{\rm me}$

Column 9: Ratio of the energy losses by synchrotron radiation to the total energy losses due to the synchrotron and inverse Compton processes, $B^2_{\rm me}/(B^2_{\rm iC} + B^2_{\rm me})$

Column 10: Ratio of the 1.4 GHz flux densities in two opposite radio lobes, S_1/S_2

Column 11: Ratio of the radio core separation from the hotspot (or the brightest region) in the brighter lobe to that from the darker one, d_2/d_1

Column 12: Misalignment angle (Δ) between straight lines connecting the core with the brightest regions in opposite lobes

The above parameters are not estimated for a few faint sample sources for which the total luminosity could not be determined because of a practically unknown radio spectrum. It is worth emphasizing that the parameters in columns 6, 7, 8, and 9 are calculated under assumptions identical to those adopted by Ishwara-Chandra & Saikia (1999) in their list of previously known giant sources. Thus, the above parameters are homogeneously determined for our giants and theirs, and can be used for statistical analyses.

6.2. Error estimates

As in Machalski & Jamrozy (2000), we have estimated the errors in the determination of $B_{\rm me}$, $u_{\rm me}$, $B_{\rm iC}/B_{\rm me}$, and $B^2_{\rm me}/(B^2_{\rm iC} + B^2_{\rm me})$ adopting errors of 20 per cent in the integral radio luminosity, and 50 per cent in the source volume. These give identical fractional errors for the

above values as follows: $B_{\rm me} \propto (1^{+0.27}_{-0.21})$, $u_{\rm me} \propto (1^{+0.60}_{-0.38})$, $B_{\rm iC}/B_{\rm me} \propto (1^{+0.21}_{-0.27})$, and $B^2_{\rm me}/(B^2_{\rm iC} + B^2_{\rm me}) \propto (1^{+0.50}_{-0.40})$.

6.3. Redshift and size estimates for identified faint galaxies

The absolute $M_{\rm R}$ magnitude of the galaxies with spectroscopic redshift varies from -22.0 mag to -25.0 mag (with the exception of J1428+2918 whose apparent R magnitude may be overestimated). A distribution of the $M_{\rm R}$ values in Table 6 has a mean of -23.65 mag and a standard deviation of 0.95 mag. Assuming this mean for the remaining identified galaxies but not observed spectroscopically (cf. Table 1), one can estimate their redshift, and hence distance, size, etc. Such estimates of redshift, logarithm of 1.4-GHz luminosity, logarithm of radio–optical luminosity ratio ($\log r$), and linear size D for the identified faint galaxies are given in columns 2, 3, 4, and 5 of Table 7. An uncertainty of the above estimates is computed taking into account the minimal and maximal $M_{\rm R}$ values as -22.0 mag and -25.0 mag. Columns 6, 7, and 8 of Table 7 give the measure of asymmetries of the sources as do columns 10, 11, and 12 of Table 6.

The size estimates of the sources in Table 7 are well above 1 Mpc, strongly suggesting that all these sources would be giants even if their host galaxy had the lowest absolute magnitude.

6.4. Remarks on some correlations between physical parameters

1) The investigated sample is inevitably biased against radio luminosity. The sources at higher redshifts (or redshift estimates) are evidently more luminous. This is not the case for the optical absolute magnitude; 11 galaxies with $0.07 < z < 0.2$ in our sample have $\langle M_{\rm R}\rangle = (-23.5 \pm 0.3)$ mag, while 7 galaxies with $0.2 < z < 0.4$ have $\langle M_{\rm R}\rangle = -(23.7 \pm 0.3)$ mag. The above parameters produce a spurious correlation between the radio–optical luminosity ratio ($\log r$) and redshift.

2) The ratio $B_{\rm iC}/B_{\rm me}$ for all the giant sources in our sample reaches the value of about 2 to 6 supporting the thesis that inverse-Compton losses are a few times larger than synchrotron radiative losses in the time evolution of the lobes of giant radio sources. Indeed, our limited data confirm the correlations between the ratio $B_{\rm iC}/B_{\rm me}$ and linear size D, as well as between $B^2_{\rm me}/(B^2_{\rm iC} + B^2_{\rm me})$ and D pointed out by Ishwara-Chandra & Saikia.

3) In most of the giant sources in Tables 6 and 7, the brighter lobe is closer to the host galaxy. This is expected if a source is intrinsically highly symmetric, its inclination angle from the observer's line of sight differs (but slightly) from 90°, and it is at an age where the luminosity of its lobes is already decreasing. In such cases, the asymmetries of the lobes in brightness and separation from the nucleus are generated by the different ages the lobes have in the observer's frame. The lobe (hotspots) seen as closer to the nucleus has to be younger and brighter than the farther one.

Acknowledgements. The authors acknowledge (i) the National Radio Astronomy Observatory (Socorro, NM) for the target-of-opportunity observing time, (ii) the McDonald Observatory (Mt. Locke, TX) for the observing time, (iii) the National Optical Astronomy Observatories (Kitt Peak, AZ) for the usage of the IRAF software, (iv) the Space Telescope Science Institute for the usage of the DSS data base, and (v) Dr Luigina Feretti for her constructive remarks improving this paper. This work was supported in part by the State Committee for Scientific Research (KBN) under contract PB 0266/PO3/99/17.

References

Blundell K.M., Rawlings S., Willott C.J., 1999, AJ 117, 677
Bruzual A.G., 1983, ApJ 273,105
Christian C.A., Adams M., Barnes J.V., et al., 1985, PASP 97, 363
Condon J.J., Cotton W.D., Greisen E.W., et al., 1998, AJ, 115, 1693 (NVSS)
Cotter G., Rawlings S., Saunders R., 1996, MNRAS 281, 1081
Eales S.A., 1985, MNRAS 217, 179
Fanaroff B.L., Riley J.M., 1974, MNRAS, 167, 31P
Hook I.M., Becker R.H., McMahon R.G., White R.L., 1998, MNRAS 297, 1115
Ishwara-Chandra C.H., Saikia D.J., 1999, MNRAS 309, 100
Jamrozy M., Machalski J., 1999, Acta Astr. 49, 181
Kaiser C.R., Dennett-Thorpe J., Alexander P., 1997, MNRAS 292, 723
Kaiser C.R., Alexander P., 1999, MNRAS 302, 515
Kennicutt R.C., 1992, ApJS 79, 255
Laing R.A., Riley J.M., Longair M.S., 1983, MNRAS 204, 151
Leahy J.P., Williams A.G., 1984, MNRAS 210,929
Machalski J., 1998, A&AS 128, 153
Machalski J., Condon J.J., 1999, ApJS 123, 41
Machalski J., Jamrozy M., 2000, A&A 363, L17
Machalski J., Jamrozy M., 2000, in "The Universe at low Radio Frequencies", ed.: A.P. Rao, ASP Conf. Series, (in **press**)
Mack K.H., Klein U., O'Dea C.P., Willis A.G., Saripalli L., 1998, A&A 329, 431
Miley G.K., 1980, ARA&A 18, 165
Rengelink R.B., Tang Y., de Bruyn A.G., et al., 1997, A&AS 124, 259
Schoenmakers A.P., Mack K.H., Lara L., et al., 1998, A&A 336, 455
Schoenmakers A.P., 1999, Ph.D Thesis, Univ. of Utrecht
Stetson P.B., 1987, PASP 99, 191
Stone R.P.S., 1977, ApJ 218, 767

Table 5. Lines detected and redshift of the galaxies

Source	Line/absorp.band detected	λ_o [Å]	z	Source	Line/absorp.band detected	λ_o [Å]	z
J0720+2837	[OII]3727	4736.7	0.2709	J1555+3653	[OII]3727	4649.8	0.2476
	CaII 3934	4998.5	0.2706		CaII 3968	4947.7	0.2469
	CaII 3968	5039.1	0.2699		G band	5365.	0.2462
	G band	5468.	0.2702		[OIII]5007	6247.0	0.2477
	[OIII]4959	6101.5	0.2707		Mg band	6456.	0.2475
	[OIII]5007	6361.6	0.2705				$\overline{0.2472} \pm 0.0007$
	Mg band	6577.	0.2709				
			$\overline{0.2705} \pm 0.0006$	J1615+3826	[OII]3727	4416.3	0.1849
					CaII 3968	4703.6	0.1854
J0912+3510	[OII]3727	4655.2	0.2491		[OIII]4959	5877.3	0.1852
	Hβ	6071.3	0.2489		[OIII]5007	5936.7	0.1857
	[OIII]4959	6192.5	0.2487				$\overline{0.1853} \pm 0.0005$
	[OIII]5007	6252.4	0.2487				
			$\overline{0.2489} \pm 0.0004$	J1635+3608	CaII 3934	4590.3	0.1668
					CaII 3968	4627.9	0.1663
J1253+4041	[OII]3727	4586.2	0.2305		G band	(5014)	(0.165)
	CaII 3934	4840.0	0.2303		Mg band	(6020)	(0.163)
	CaII 3968	4881.8	0.2303		Na D	6875.	0.1666
	G band	5295.	0.2300				$\overline{0.1655} \pm 0.0015$
	[OIII]4959	6098.7	0.2298				
	[OIII]5007	6158.3	0.2299	J1018–1240	CaII 3934	4237.8	0.0772
	Mg band	6367.	0.2303		CaII 3968	4278.6	0.0783
	Na D	7248.	0.2299		G band	4641.	0.0781
			$\overline{0.2302} \pm 0.0005$		Mg band	5580.	0.0783
					Na D	6350.	0.0775
J1343+3758	[OIII]4959	6083.1	0.2267		Hα	7065.9	0.0768
	[OIII]5007	6141.7	0.2266				$\overline{0.0777} \pm 0.0007$
			$\overline{0.2267} \pm 0.0005$				
				J1218+5026	[OII]3727	4470.4	0.1995
J1344+4028	CaII 3934	4223.3	0.0735		[NeIII]3869	4640.9	0.1995
	CaII 3968	4257.7	0.0730		Hγ+[OIII]	5205.	0.199
	G band	4620.	0.0732		Hβ	5831.7	0.1997
	Mg band	5580.	0.0783		[OIII]4959	5948.5	0.1995
	Na D	6340.	0.0759		[OIII]5007	6005.8	0.1995
			$\overline{0.075} \pm 0.002$				$\overline{0.1995} \pm 0.0004$
J1345+3952	CaII 3934	4567.7	0.1611	J1328–0307	[OIII]4959	5387.1	0.0863
	CaII 3968	4607.9	0.1613		[OIII]5007	5437.6	0.0860
	G band	5000.	0.1614		Hα	7125.3	0.0858
	Mg band	6003.	0.1601				$\overline{0.0860} \pm 0.0005$
	Na D	6846.	0.1617				
			$\overline{0.1611} \pm 0.0008$	J1457–0613	[OII]3727	4350.2	0.1672
					Hβ	5674.4	0.1673
J1451+3357	[OII]3727	4940.7	0.3257		[OIII]4959	5787.2	0.1670
	Hβ	6441.5	0.3251		[OIII]5007	5842.7	0.1669
	[OIII]4959	6599.9	0.3248				$\overline{0.1671} \pm 0.0002$
	[OIII]5007	6632.9	0.3247				
			$\overline{0.3251} \pm 0.0005$				
J1512+3050	CaII 3934	4284.8	0.0892				
	G band	4690.	0.0894				
	Mg band	5640.	0.0899				
	Na D	6421.	0.0896				
			$\overline{0.0895} \pm 0.0006$				

Table 6. Physical parameters of the sources with spectroscopic redshift

Source	$\log L_{1.4}$ [W/Hz]	$M_{\rm R}$ [mag]	$\log r$	D [Mpc]	$B_{\rm me}$ [nT]	$u_{\rm me}\,10^{-13}$ [erg/cm^3]	$\frac{B_{iC}}{B_{me}}$	$\frac{B^2_{me}}{B^2_{iC}+B^2_{me}}$	S_1/S_2	d_2/d_1	Δ [°]
J0720+2837	25.19	–24.4	1.9	1.91					0.9	1.38	2
J0912+3510	25.65	–22.5	3.1	1.84	0.112	1.16	4.5	0.047	(0.6)	(1.60)	(2)
		.....	....	.....					(1.8)	(1.35)	(1)
J1113+4017	24.78	–23.9	1.7	1.38	0.166	2.56	2.2	0.165	1.6	.....	...
J1218+5026	26.03	–23.4	3.2	0.81	0.356	11.80	1.3	0.370	1.3	0.71	
J1253+4041	25.11	–24.3	1.9	1.28	0.086	0.69	5.7	0.030	1.7	1.10	1
J1343+3758	25.52	–23.6	2.6	3.14	0.083	0.63	5.9	0.028	1.5	1.34	3
J1344+4028	24.74	–23.6	1.8	0.86							
J1345+3952	25.32	–24.7	1.9	0.60	0.190	3.33	2.3	0.159	1.2	1.24	5
J1428+2918	25.16	–25.8	1.3	1.98						0.86	5
J1445+3051	25.90	–25.0	2.4	1.91	0.148	2.05	4.4	0.049	1.6	1.35	0
J1451+3357	25.84	–24.2	2.6	1.41	0.145	1.95	3.9	0.061	1.2	1.22	4
J1453+3309	26.14	–23.6	3.2	1.57	0.197	3.59	2.6	0.132	1.6	1.65	12
J1512+3050	24.60	–22.9	1.9	0.54					1.1	1.10	5
J1555+3653	25.49	–23.3	2.7	1.63						1.12	0
J1604+3731	26.67	?	3.7–3.9	1.50	0.289	7.73	3.7	0.068	1.5	1.05	5
J1615+3826	24.74	–23.3	1.9	0.98					1.1	.....	...
J1635+3608	25.09	–23.3	2.3	1.18	0.090	0.75	4.9	0.040	....	.....	...
J1018–1240	24.88	–22.2	2.5	1.10					....	.....	...
J1328–0307	24.83	–22.0	2.5	1.75					....	1.15	5
J1457–0613	25.82	–23.3	3.0	0.87					....	1.30	0

Table 7. Probable physical parameters of the giant candidates with photometric redshift estimates derived with the assumption of $M_{\rm R} = (-23.65^{+1.65}_{-1.35})$ mag

Source	$(z \pm \Delta z)_{\rm est}$	$\log L_{1.4}$ [W/Hz]	$\log r$	D [Mpc]	S_1/S_2	d_2/d_1	Δ [°]
J0927+3510	$0.45^{+0.13}_{-0.17}$	$26.0^{+0.3}_{-0.4}$	3.1	$2.3^{+0.3}_{-0.5}$		(1.90)	(4)
	$0.55^{+0.12}_{-0.15}$	$26.2^{+0.2}_{-0.3}$	3.2	$2.5^{+0.2}_{-0.3}$		(0.99)	(1.5)
J1011+3111	$0.50^{+0.13}_{-0.15}$	$25.9^{+0.2}_{-0.3}$	3.0	$2.0^{+0.2}_{-0.3}$	1.2	1.04	5
J1155+4029	$0.53^{+0.12}_{-0.15}$	$26.7^{+0.2}_{-0.3}$	3.7	$1.7^{+0.1}_{-0.2}$	6.5	1.95	2
J1200+3449	$0.50^{+0.13}_{-0.15}$	$26.5^{+0.2}_{-0.4}$	3.6	$1.0^{+0.1}_{-0.1}$	1.9	1.32	7
J1254+2933	$0.42^{+0.12}_{-0.14}$	$25.7^{+0.2}_{-0.4}$	2.7	$2.0^{+0.2}_{-0.4}$	1.9	1.24	1.5
J1355+2923	$0.43^{+0.12}_{-0.14}$	$26.2^{+0.2}_{-0.4}$	3.2	$1.7^{+0.2}_{-0.3}$	1.2	1.05	0
J1525+3345	$0.47^{+0.12}_{-0.14}$	$25.8^{+0.2}_{-0.3}$	2.8	$1.5^{+0.1}_{-0.2}$	2.3	1.03	3
J1554+3945	$0.35^{+0.12}_{-0.13}$	$25.6^{+0.3}_{-0.4}$	2.7	$1.3^{+0.2}_{-0.3}$	1.1	1.12	2
J1649+3114	$0.36^{+0.12}_{-0.13}$	$26.0^{+0.3}_{-0.4}$	3.0	$1.3^{+0.2}_{-0.3}$		1.61	1
J1712+3558	$0.32^{+0.11}_{-0.12}$	$25.6^{+0.3}_{-0.4}$	2.7	$1.2^{+0.2}_{-0.3}$	3.3	1.34	1
J1725+3923	$0.29^{+0.11}_{-0.11}$	$25.6^{+0.3}_{-0.4}$	2.6	$1.5^{+0.2}_{-0.4}$	0.8	1.36	1

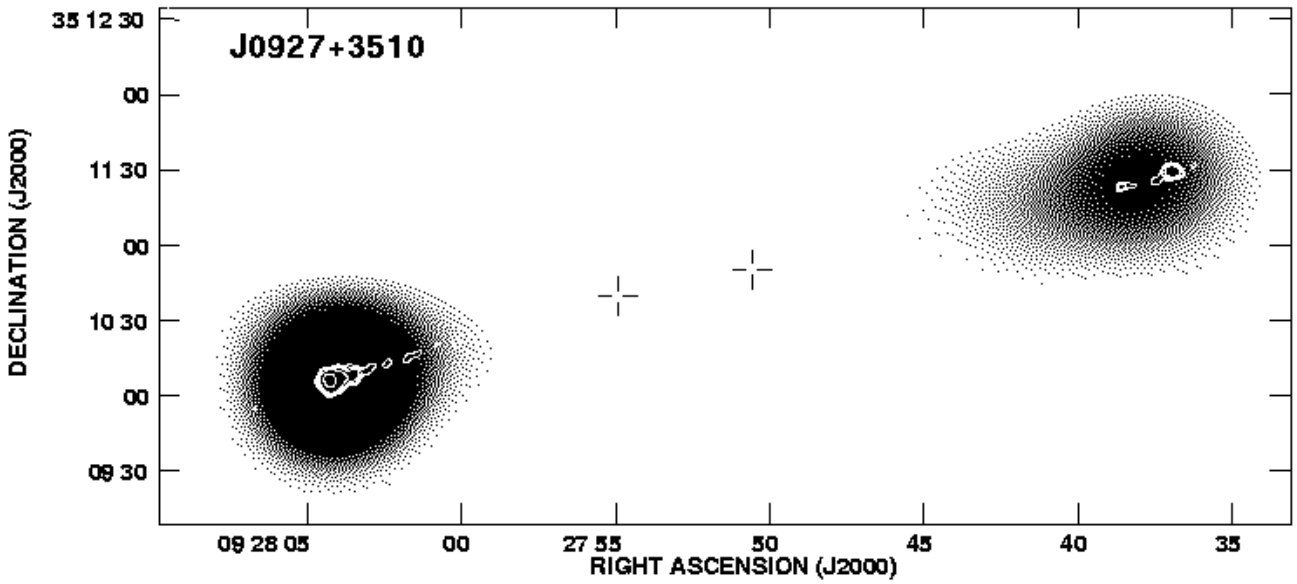

Fig. 1a. 8.46-GHz VLA map of the source J0927+3510 with no radio core detected (white contours) overlayed on 1.4-GHz NVSS map (gray scale). The crosses indicate positions of the two galaxies given in Table 4 and shown in Fig. 3b

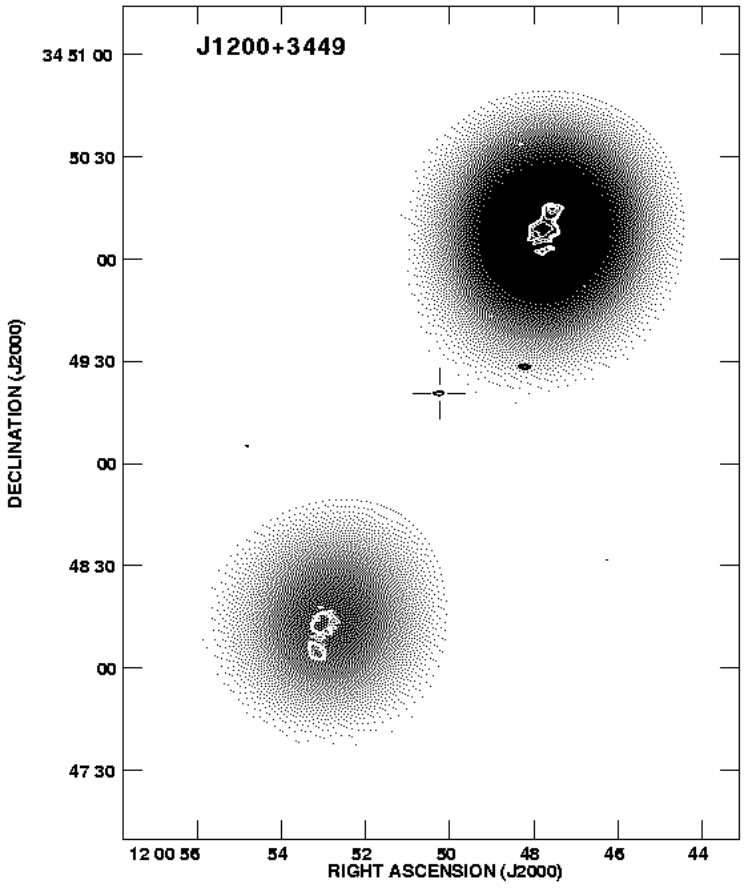

Fig. 1b. The same as in Fig. 1a but for the source J1200+3449. The radio core detected is marked by black contours. The cross indicates position of the identified galaxy (cf. Table 4)

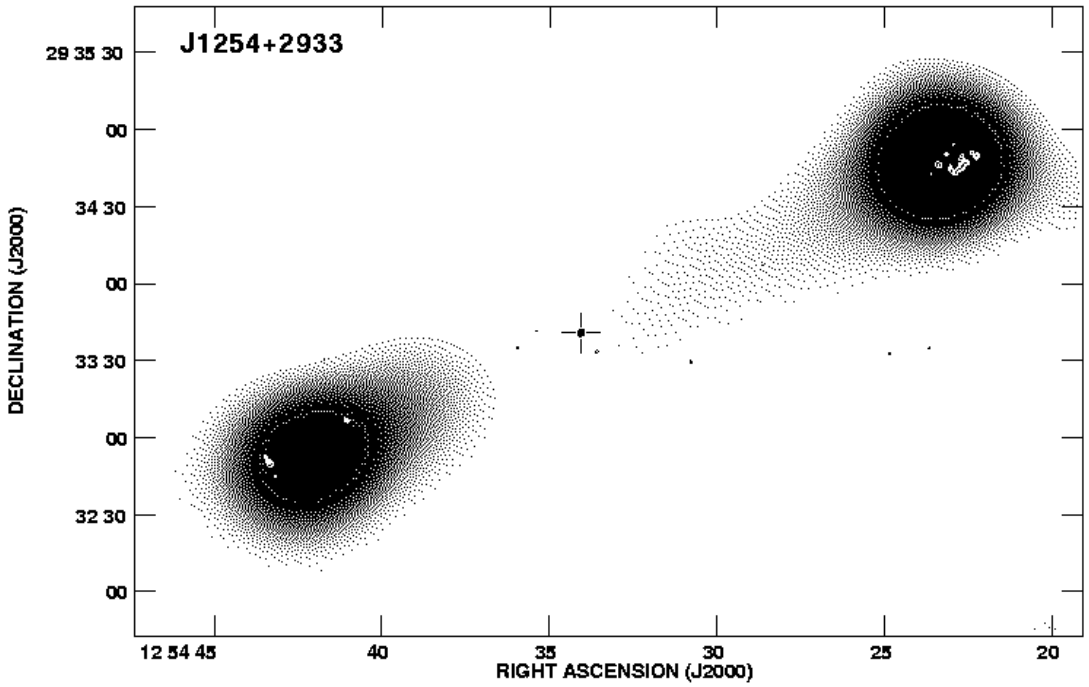

Fig. 1c. 4.86-GHz VLA map of the source J1254+2933 (white contours) overlayed on the NVSS map (gray scale). The cross indicates position of the radio core and the identified galaxy

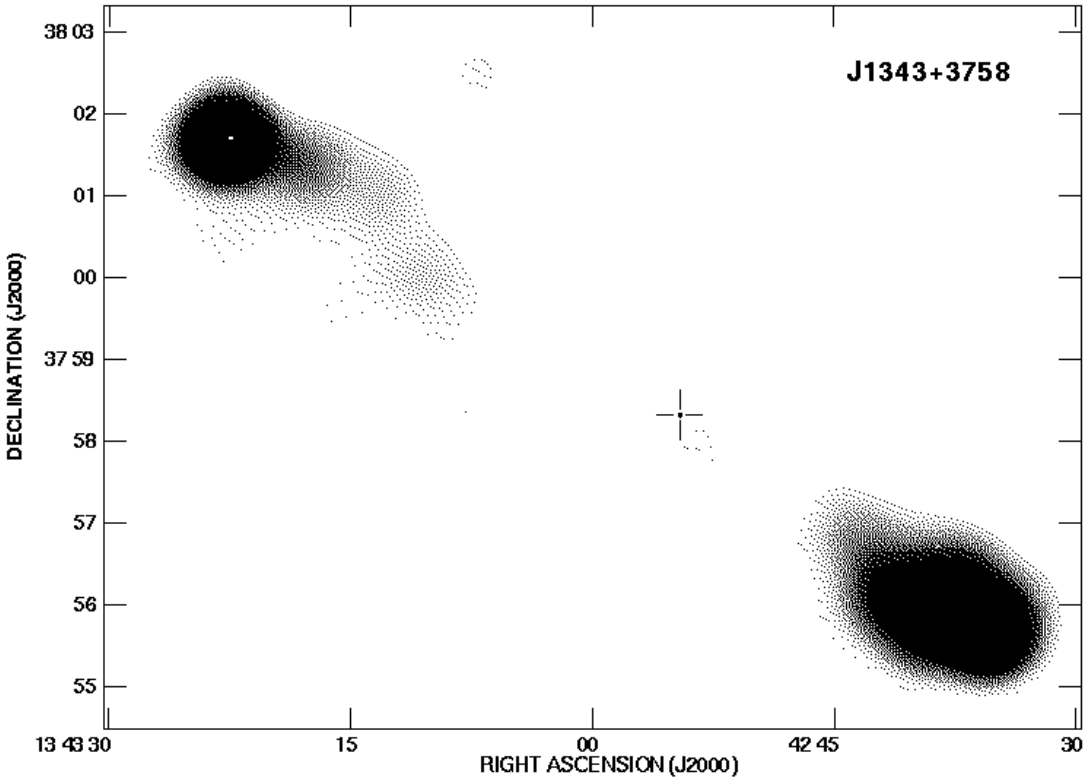

Fig. 1d. As in Fig. 1c but for the source J1343+3758

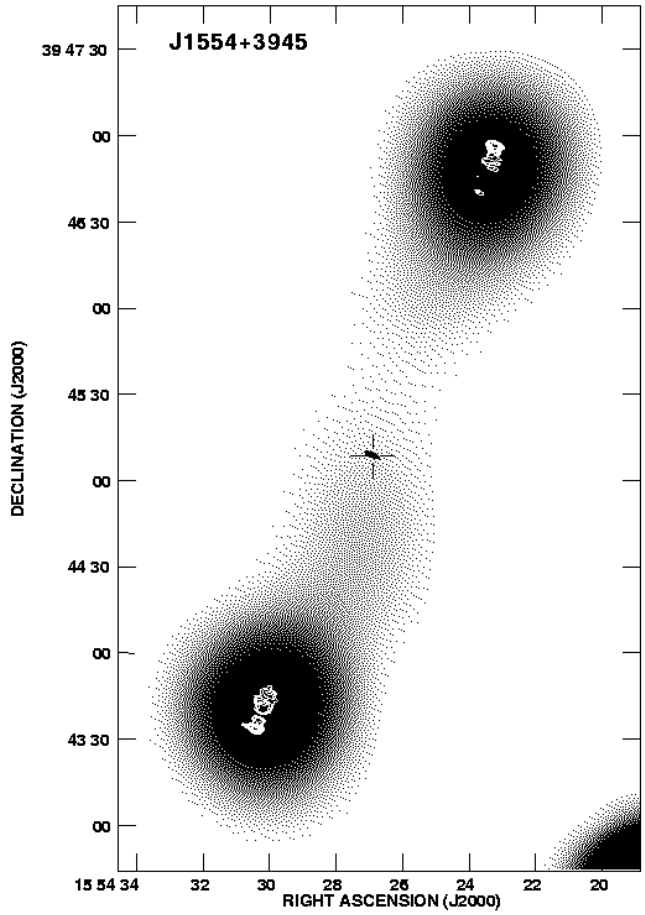

Fig. 1e. As in Fig. 1c but for the source J1554+3945

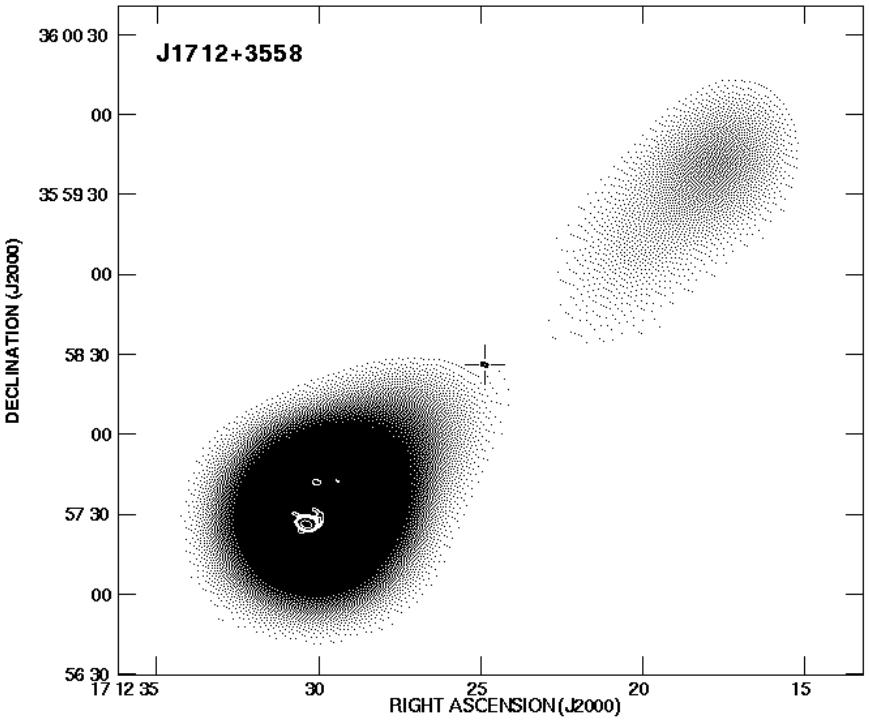

Fig. 1f. As in Fig. 1c but for the source J1712+3558

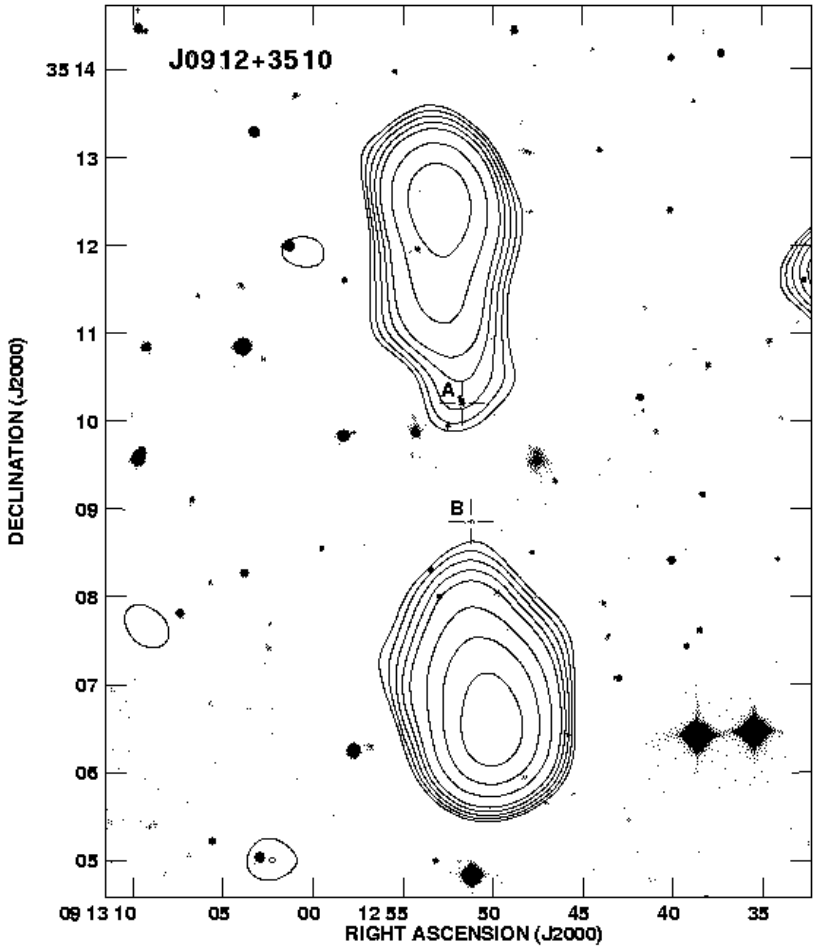

Fig. 2a. NVSS contour map of the source 0912+3510 overlayed on the optical DSS image indicating the galaxies given in Table 4

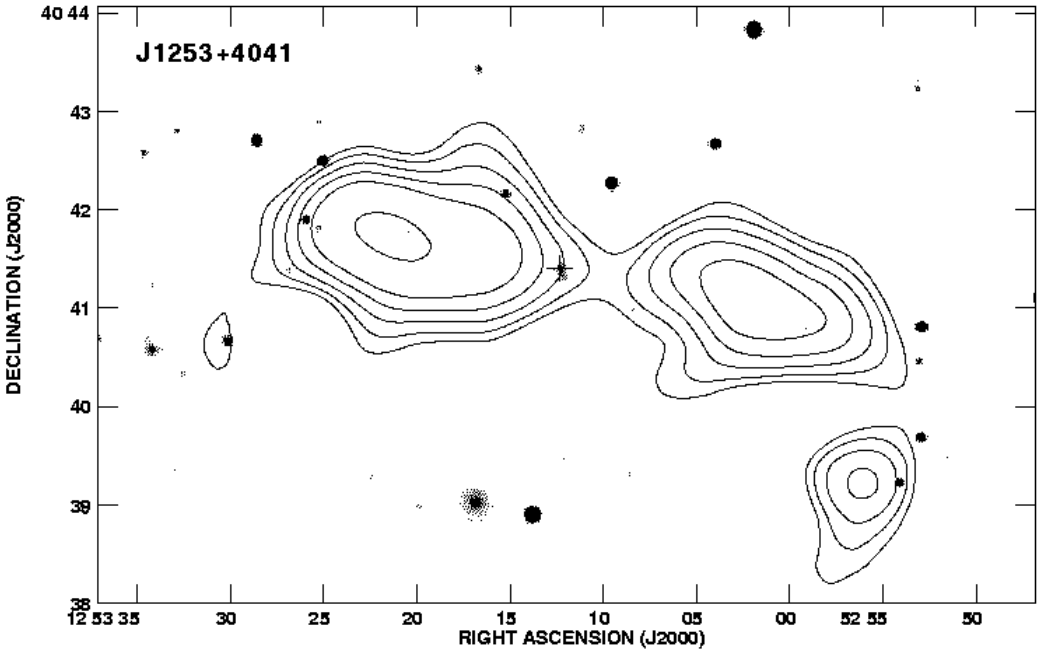

Fig. 2b. NVSS contour map of the source J1253+4041 overlayed on the optical DSS image indicating the galaxy (cross) whose spectrum in shown in Fig. 4e

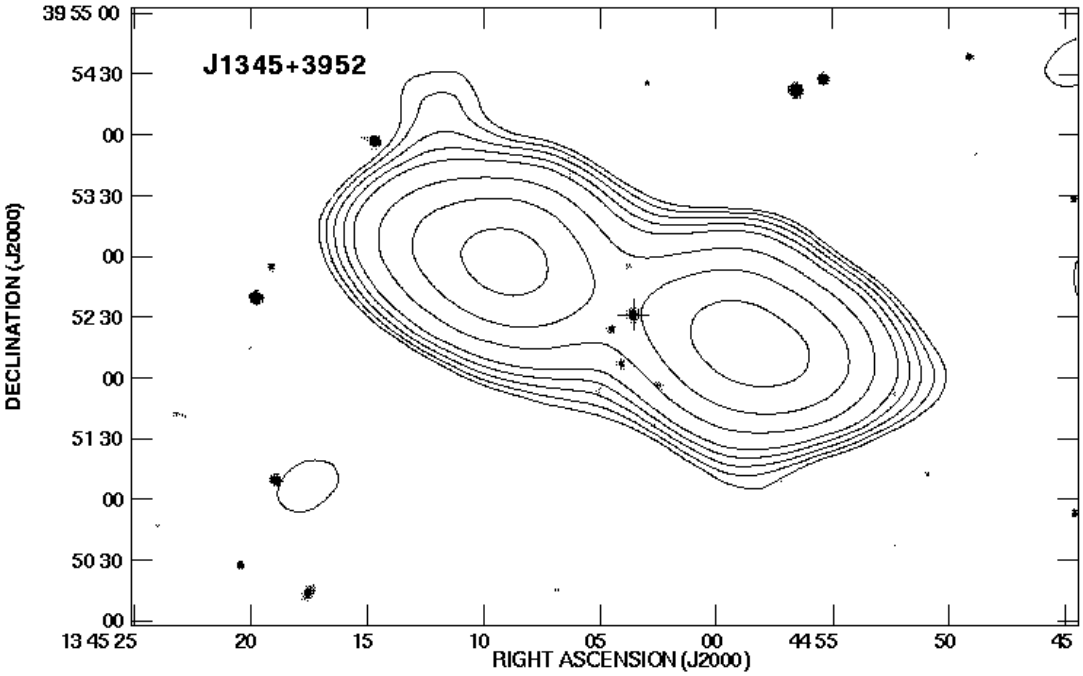

Fig. 2c. As in Fig. 2b but for the source J1345+3952. The spectrum of the galaxy marked with the cross is shown in Fig. 4i

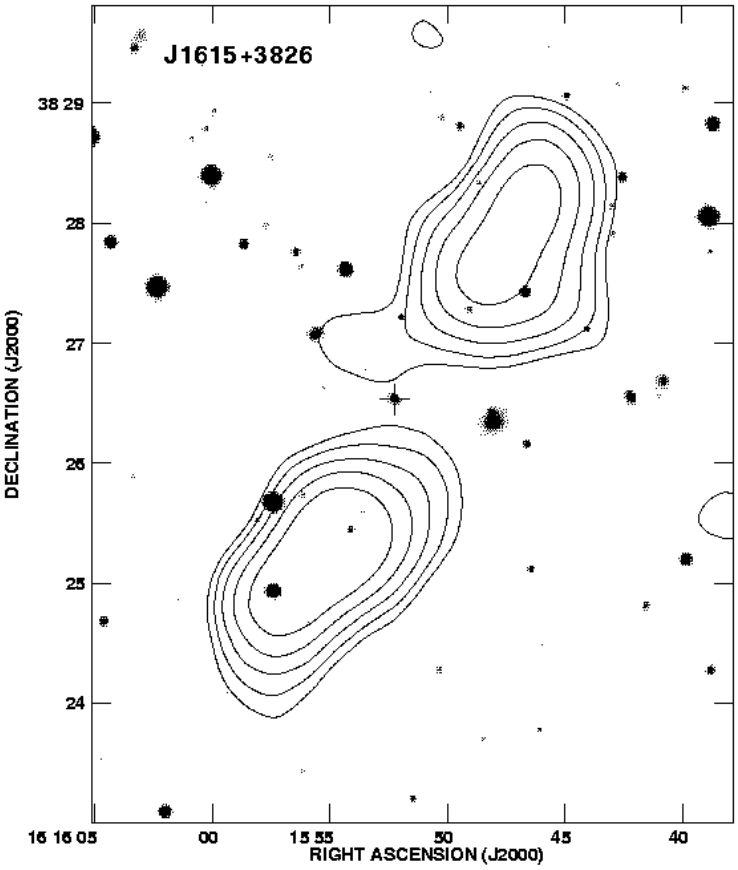

Fig. 2d. As in Fig. 2b but for the source J1615+3826. The spectrum of the galaxy marked with the cross is shown in Fig. 4n

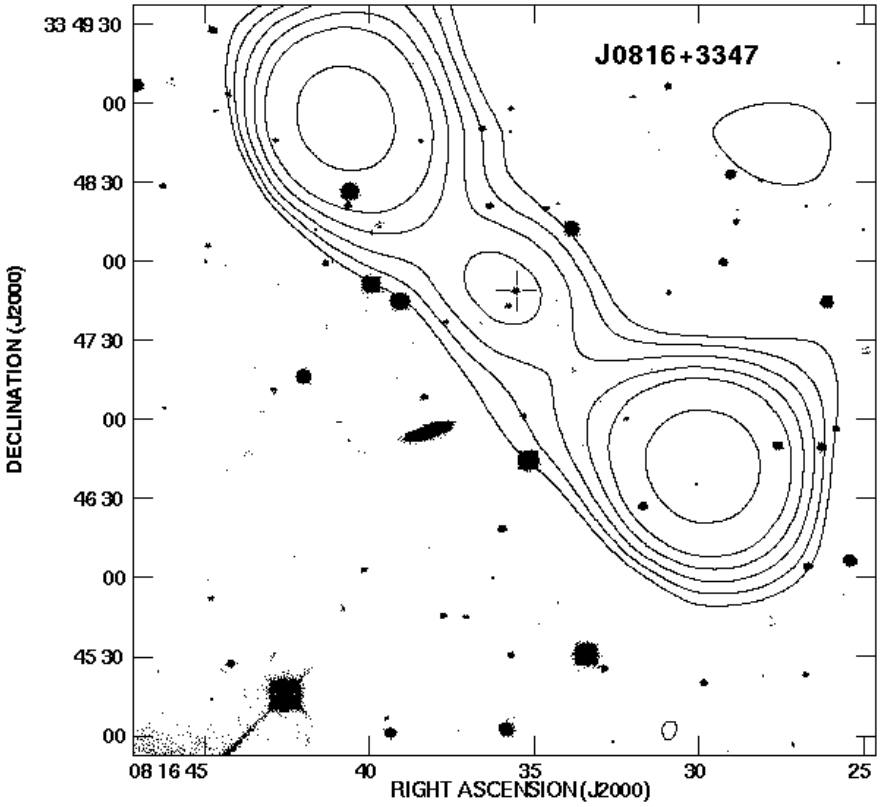

Fig. 3a. Deep R-band image of the optical field around the source J0816+3347. The host optical object (possibly a quasar) is marked with the cross. The NVSS contour map is overlayed for a comparison

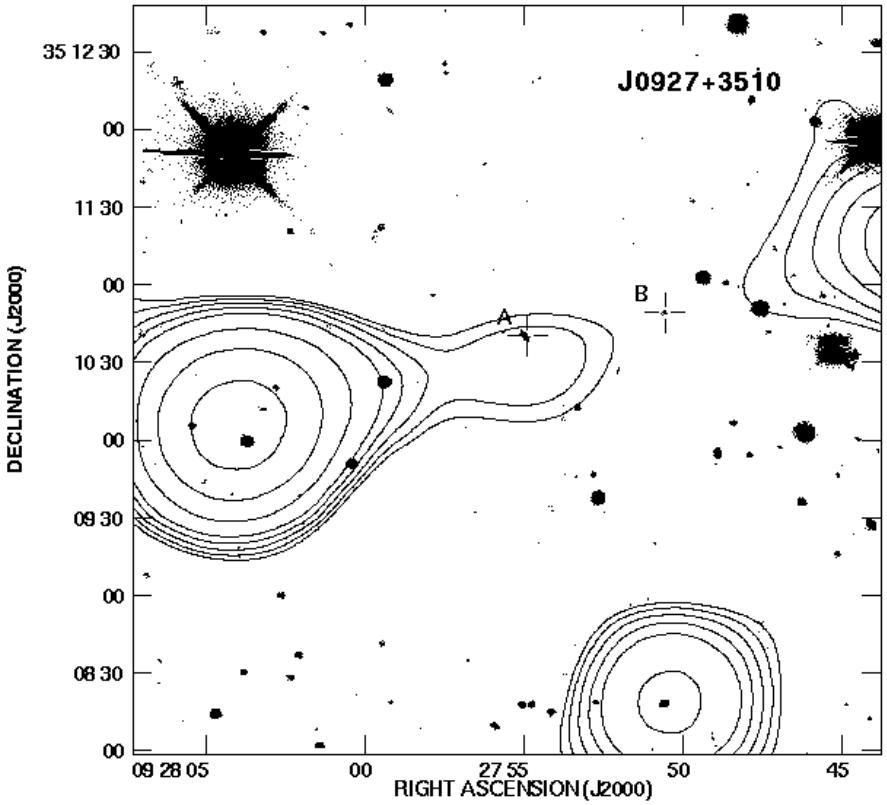

Fig. 3b. As in Fig. 3a but around the source J0927+3510. The two galaxies listed in Table 4 are marked with the crosses

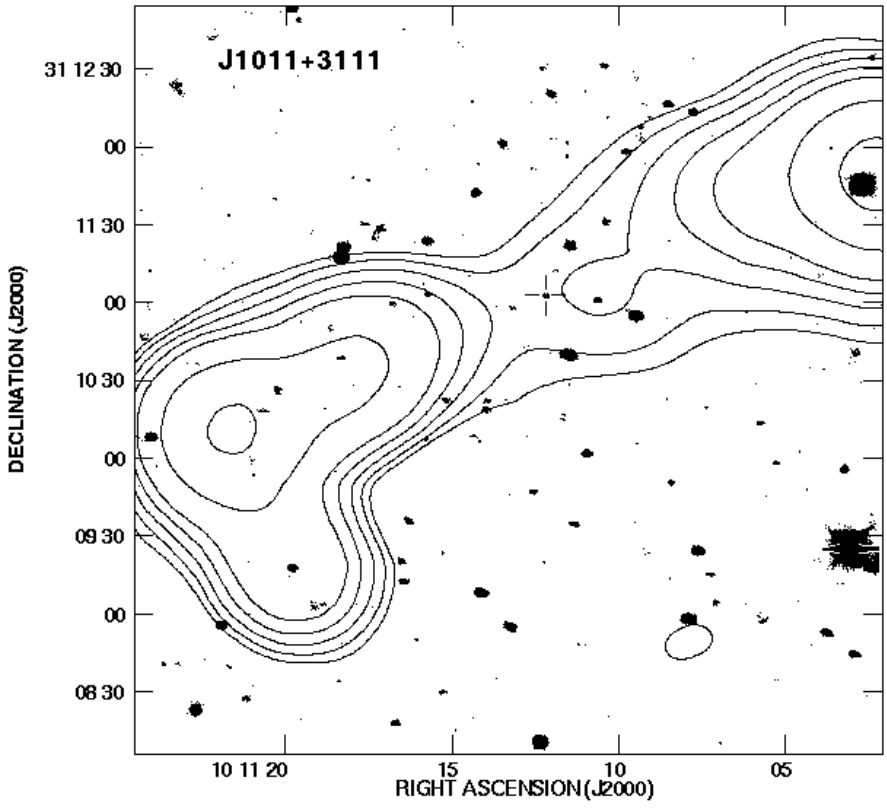

Fig. 3c. As in Fig. 3a but around the source J1011+3111. The identified 21.2 mag galaxy in marked with the cross

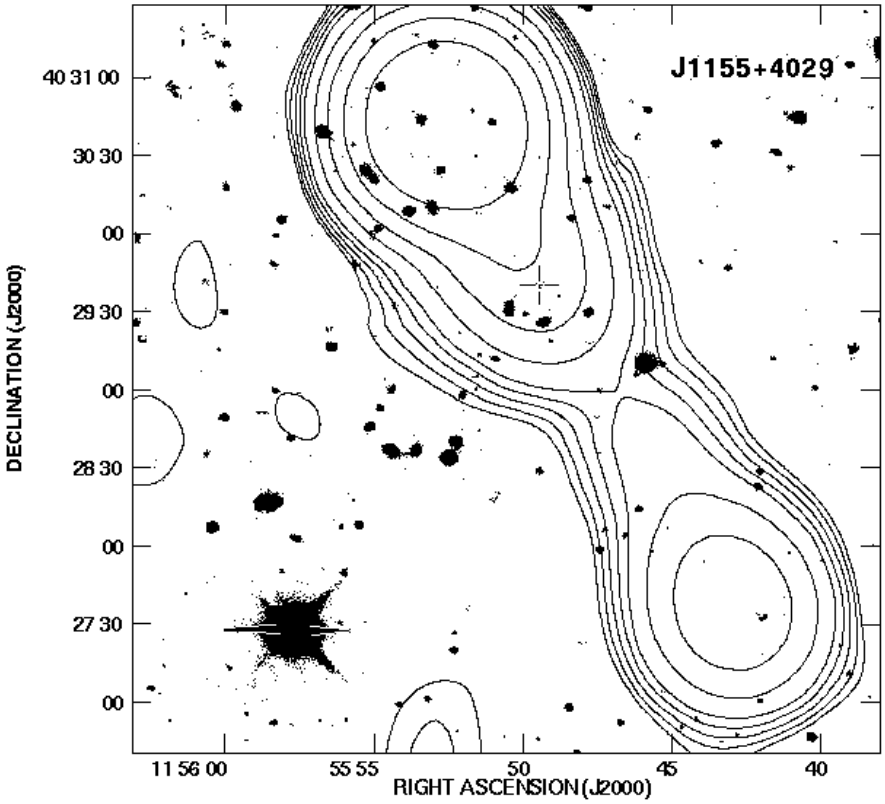

Fig. 3d. As in Fig. 3a but around the source J1155+4029. The identified 21.5 mag galaxy is marked with the cross

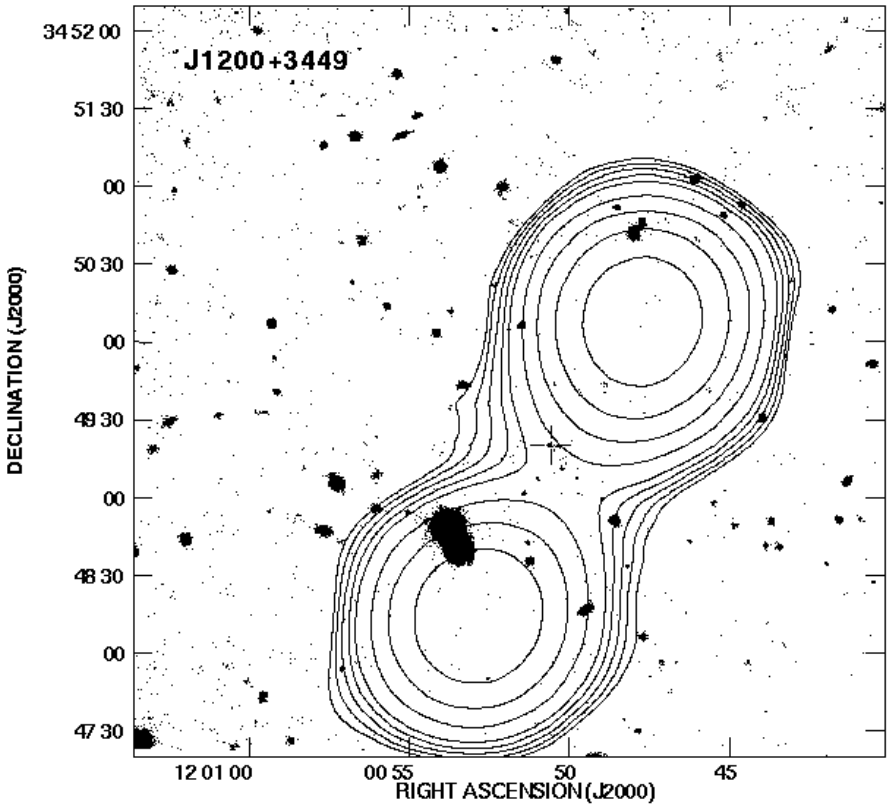

Fig. 3e. As in Fig. 3a but around the source J1200+3449. The identified 21.2 mag galaxy and the radio core (cf. Fig. 1b) are deflected from the axis of radio cocoon suggested by the NVSS contour map overlayed

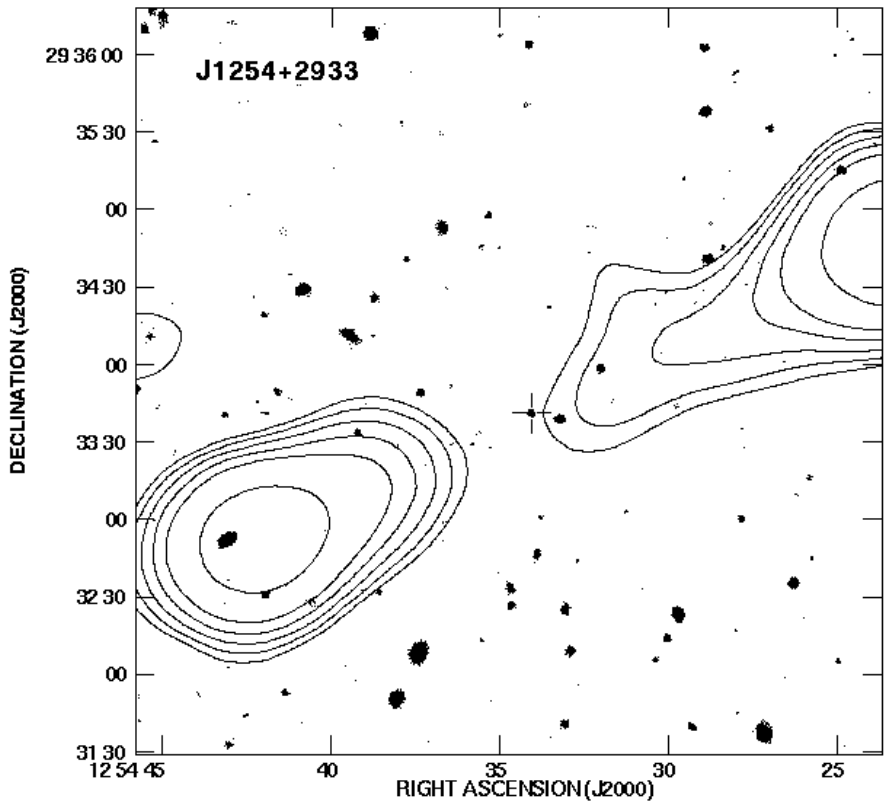

Fig. 3f. As in Fig. 3a but around the source J1254+2933. The identified 20.3 mag galaxy is marked with the cross

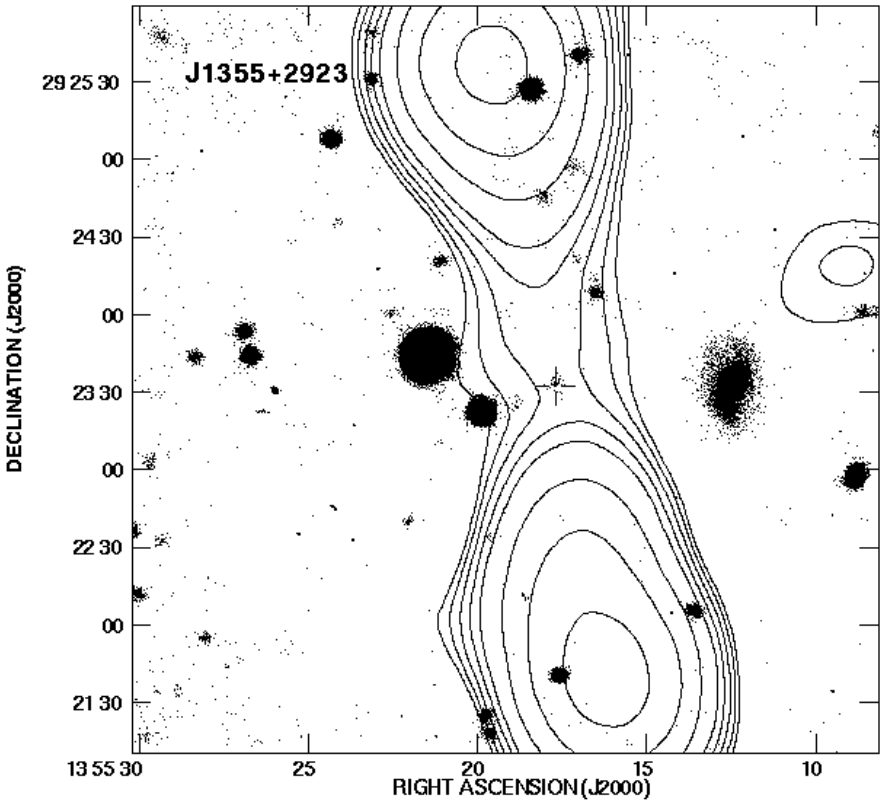

Fig. 3g. As in Fig. 3a but around the source J1355+2923. The identified 20.4 mag galaxy is marked with the cross

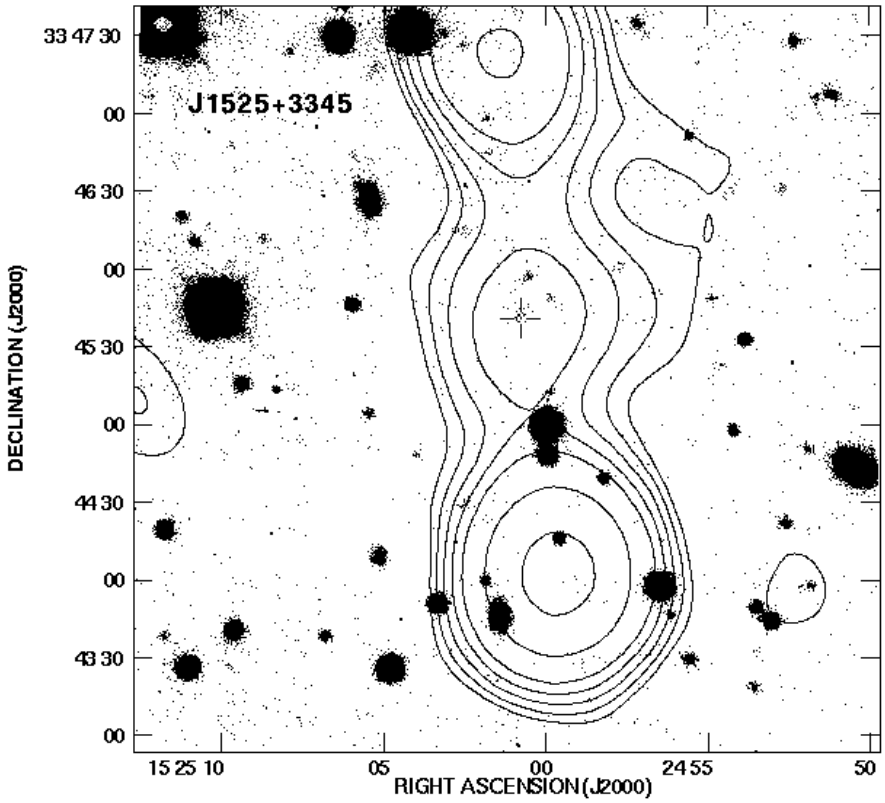

Fig. 3h. As in Fig. 3a but around the source J1525+3345. The identified 20.9 mag galaxy is marked with the cross

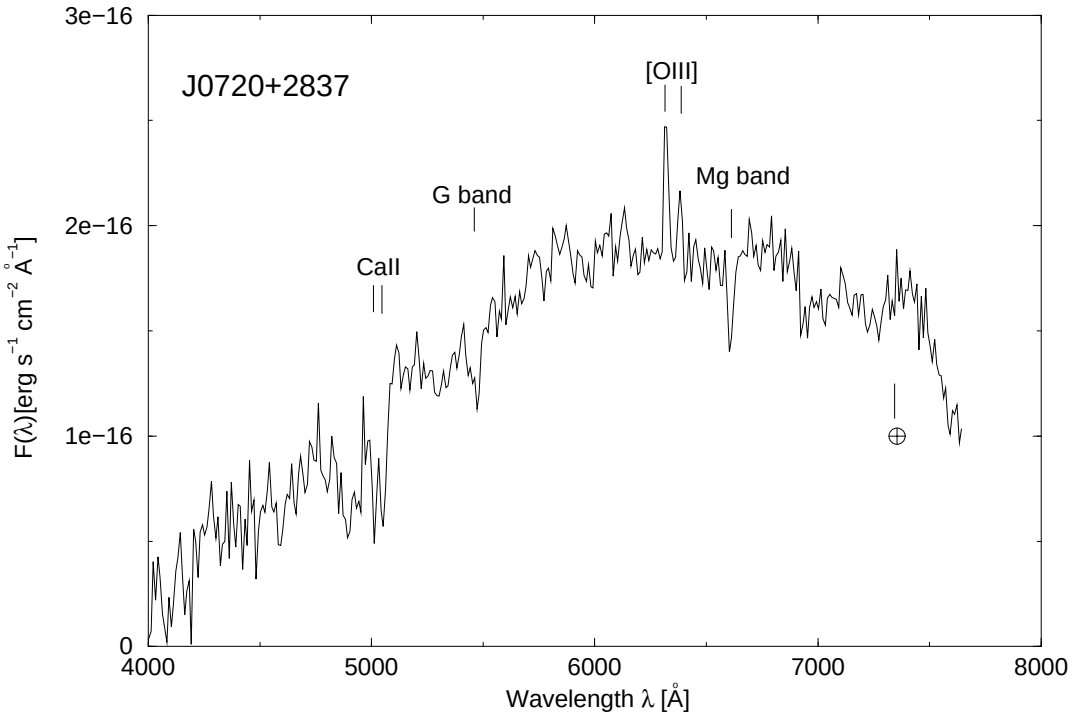

Fig. 4a. Optical spectrum of the galaxy identified with the source J0720+2837

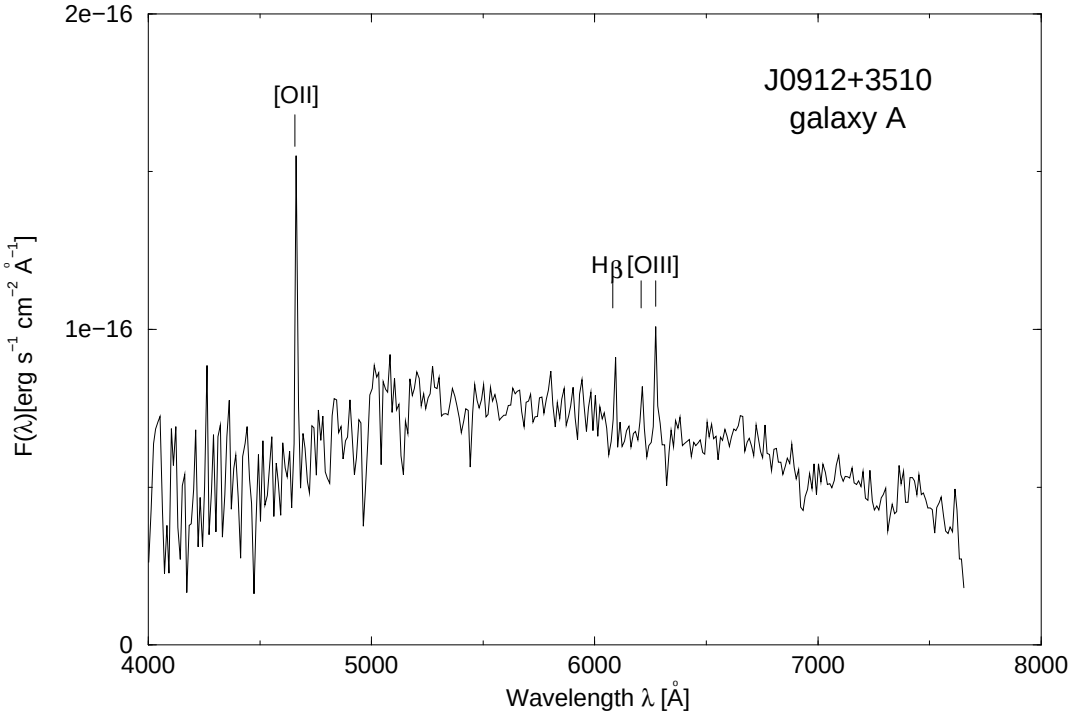

Fig. 4b. Optical spectrum of the galaxy A, a possible identification of the source J0912+3510

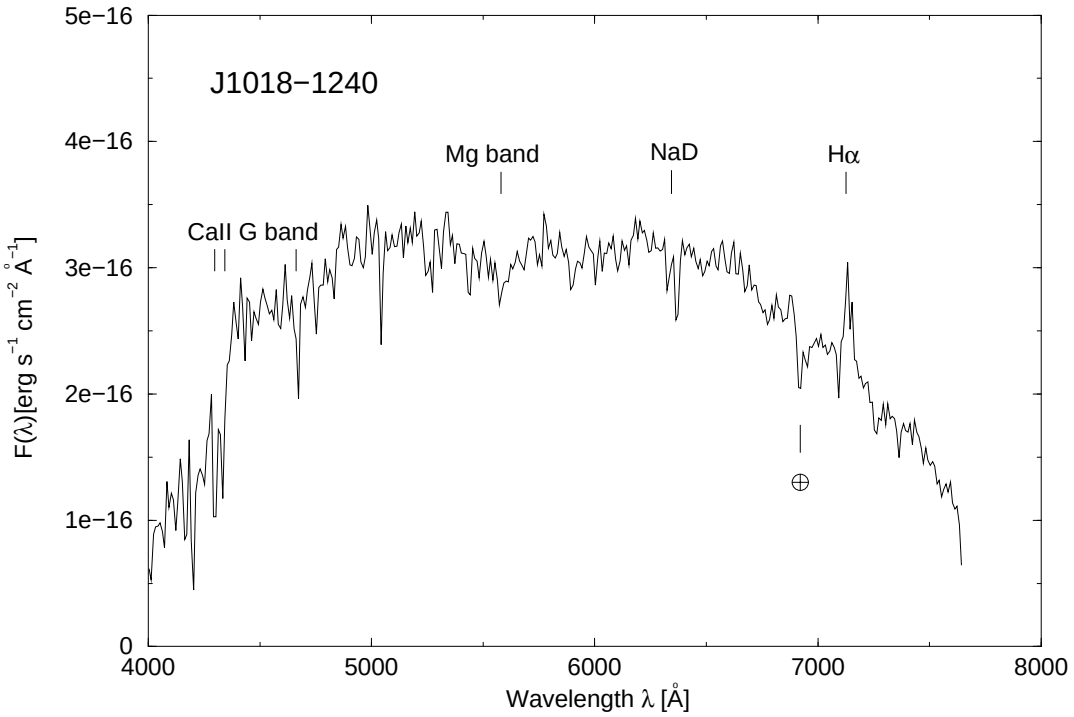

Fig. 4c. As in Fig. 4a but for the galaxy identified with the source J1018–1240

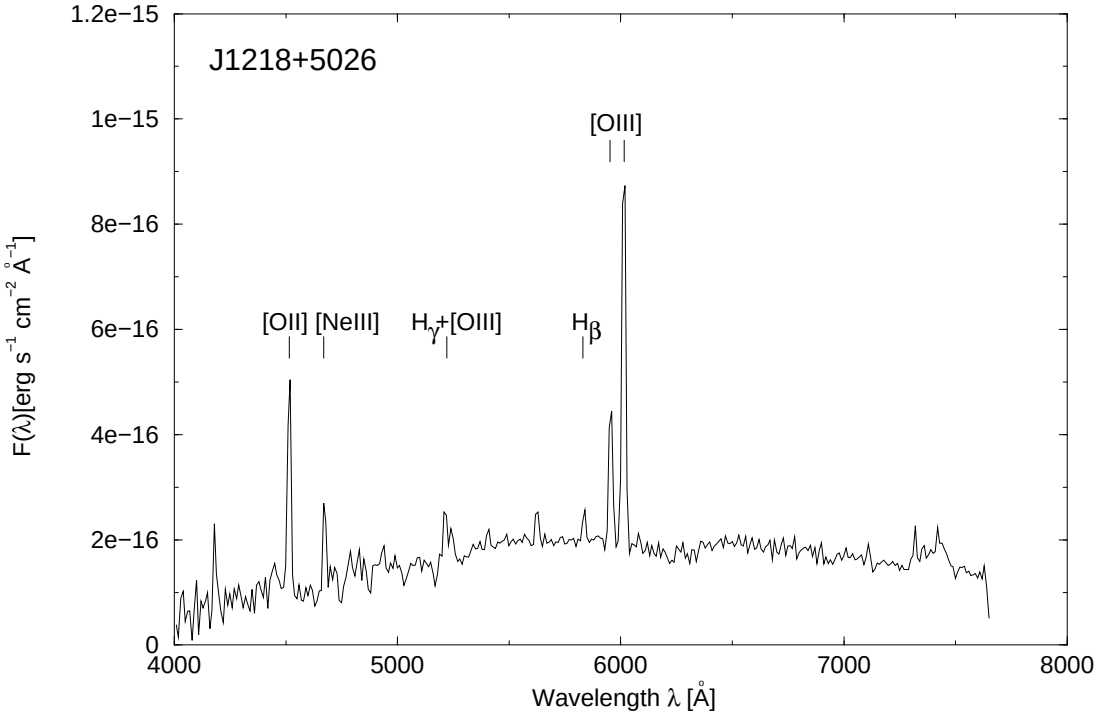

Fig. 4d. As in Fig. 4a but for the galaxy identified with the source J1218+5026

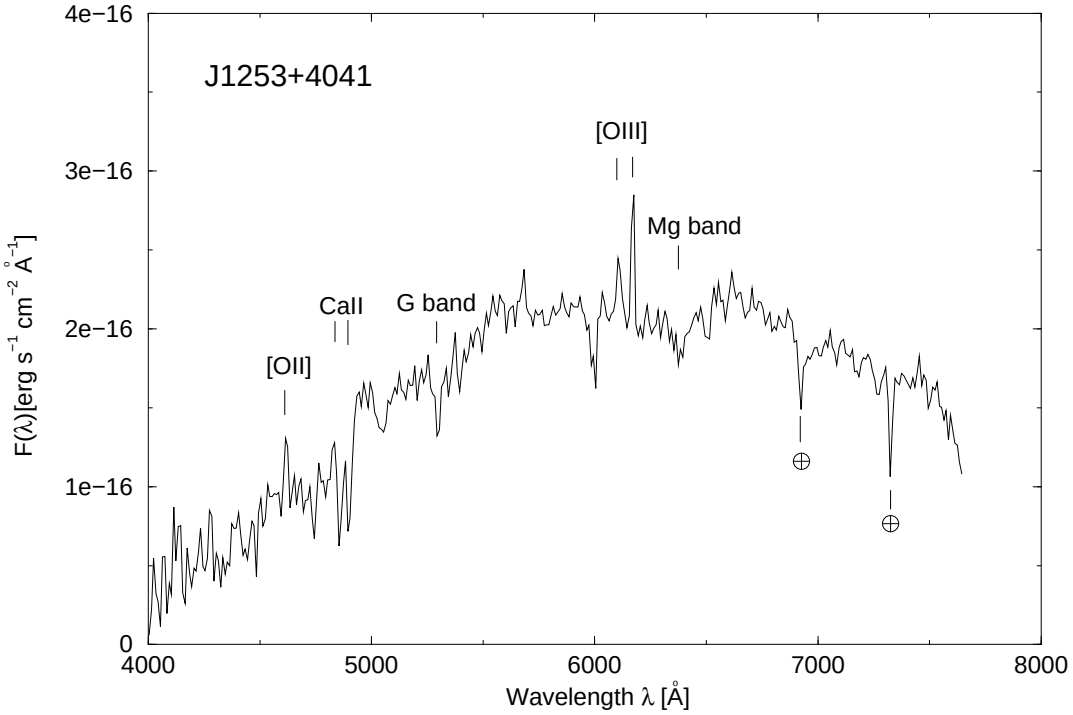

Fig. 4e. As in Fig. 4a but for the galaxy likely identified with the source J1254+4041

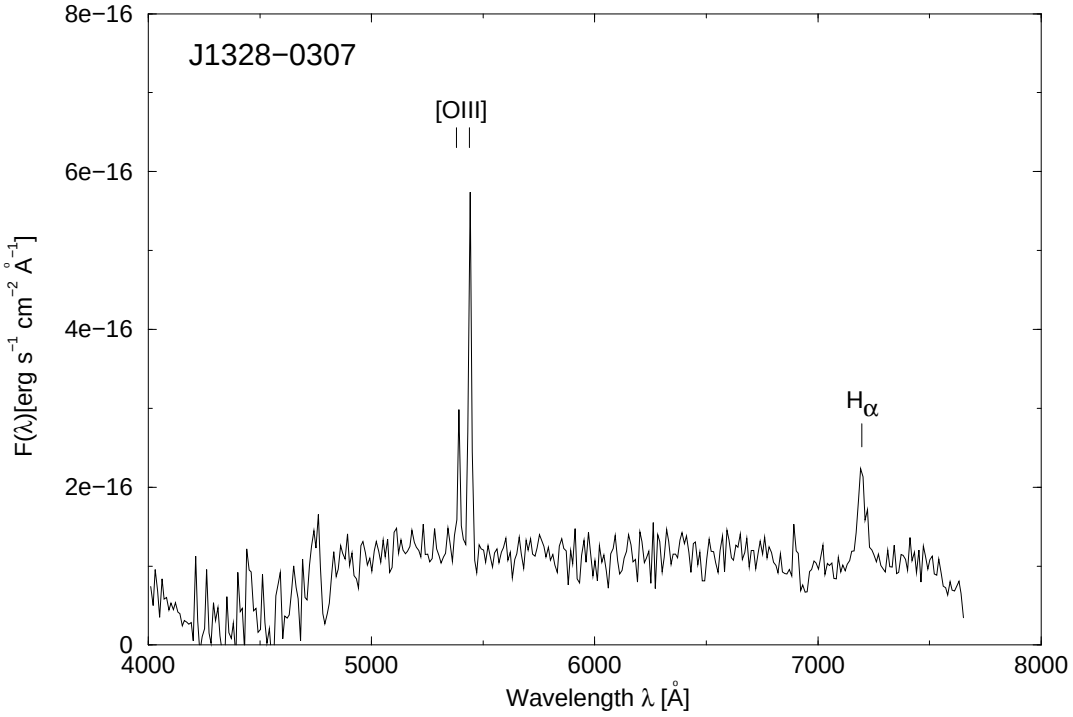

Fig. 4f. As in Fig. 4a but for the galaxy identified with the source J1328–0307

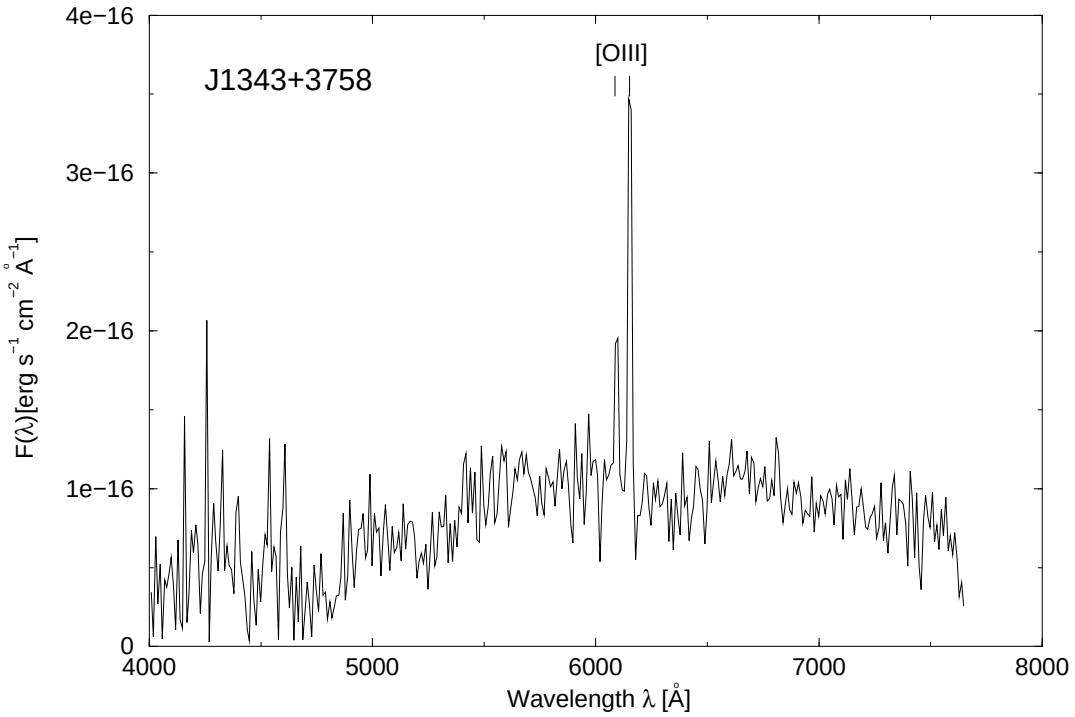

Fig. 4g. As in Fig. 4a but for the galaxy identified with the source J1343+3758

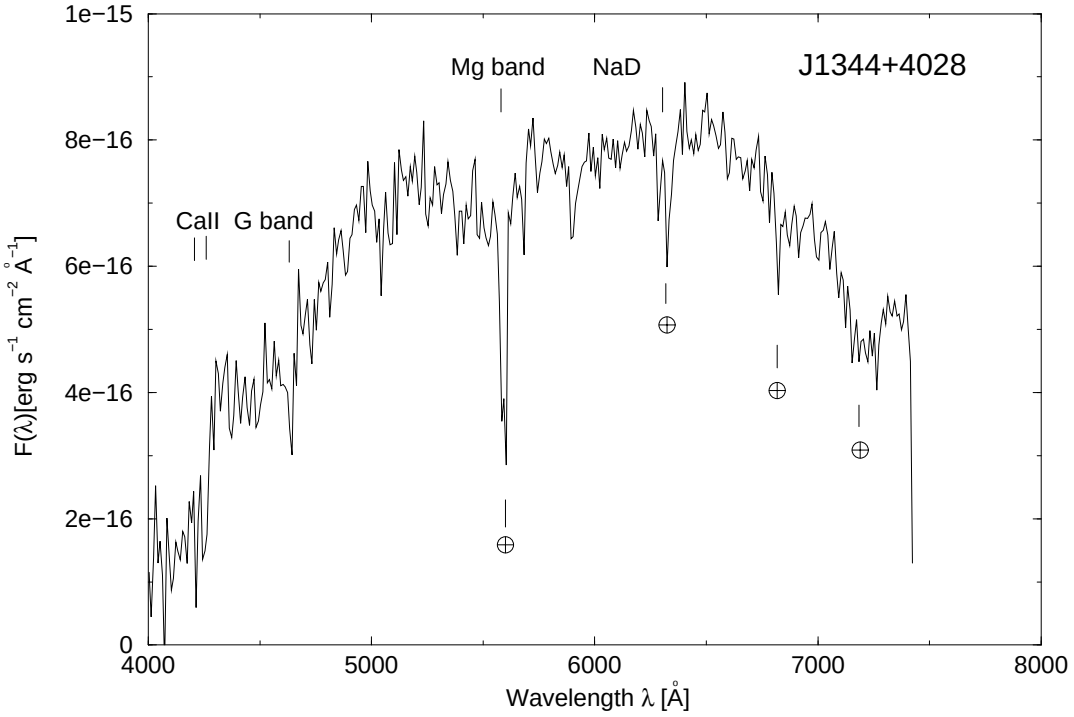

Fig. 4h. As in Fig.4a but for the galaxy identified with the source J1344+4028

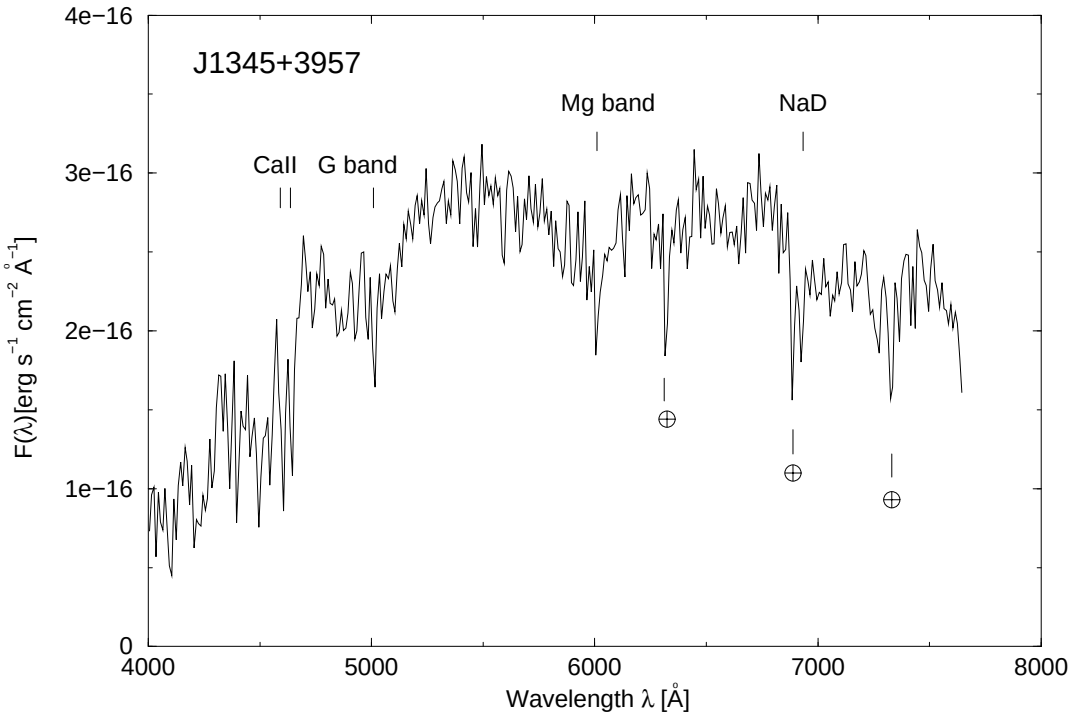

Fig. 4i. As in Fig. 4a but for the galaxy likely identified with the source J1345+3952

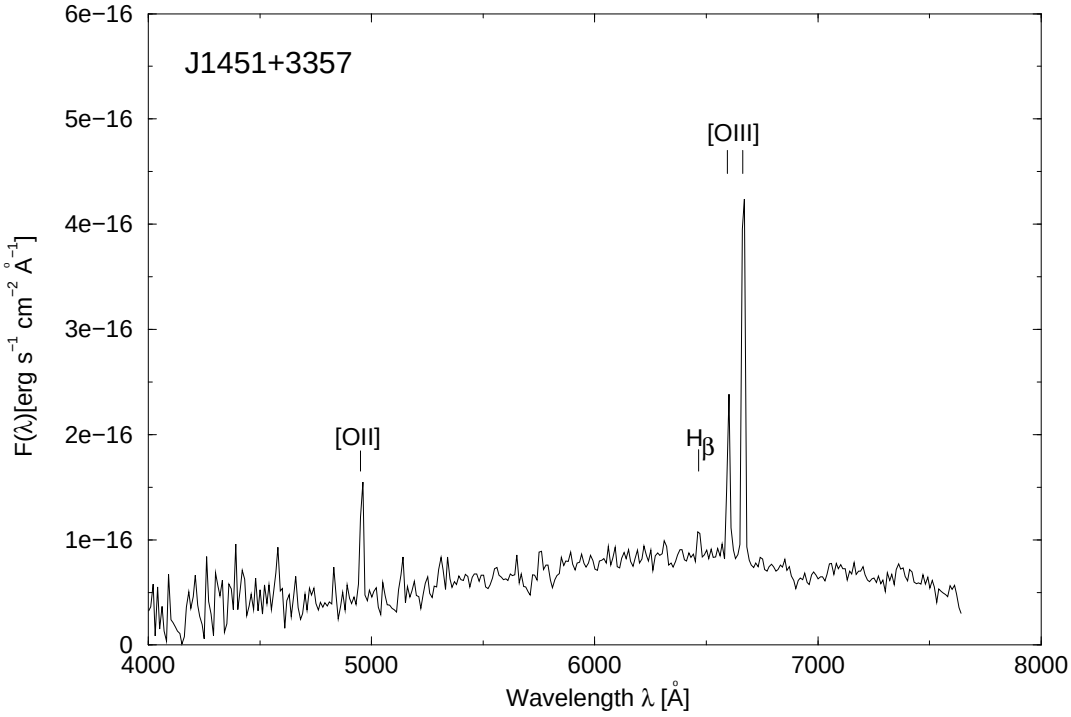

Fig. 4j. As in Fig. 4a but for the galaxy identified with the source J1451+3357

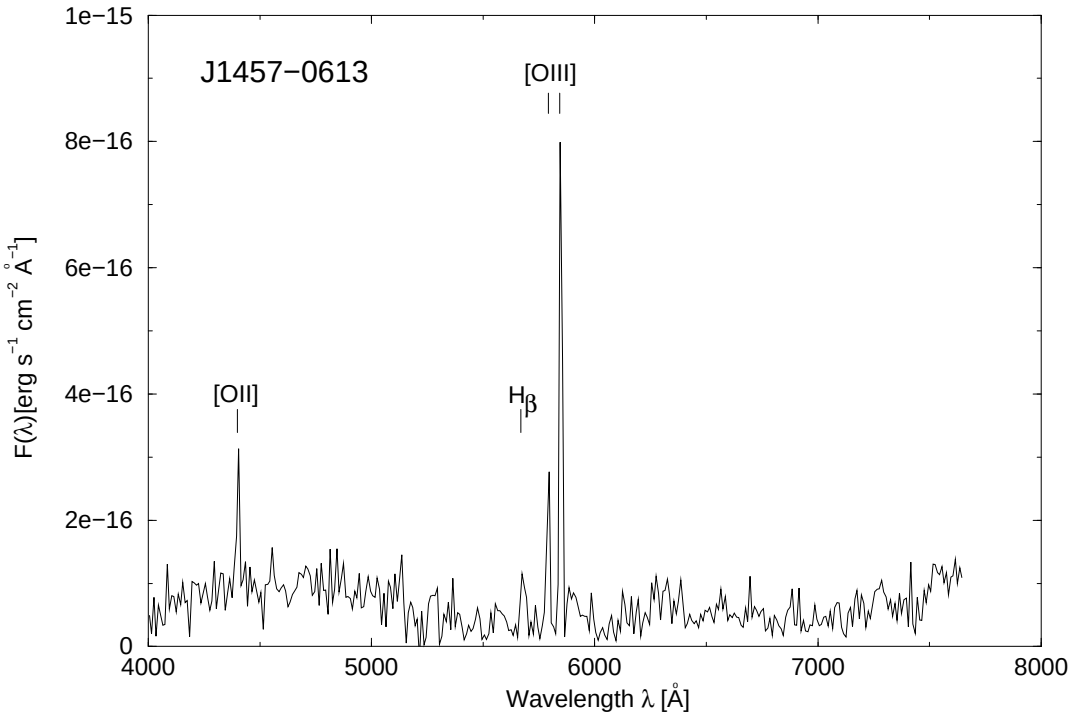

Fig. 4k. As in Fig. 4a but for the galaxy identified with the source J1457–0613

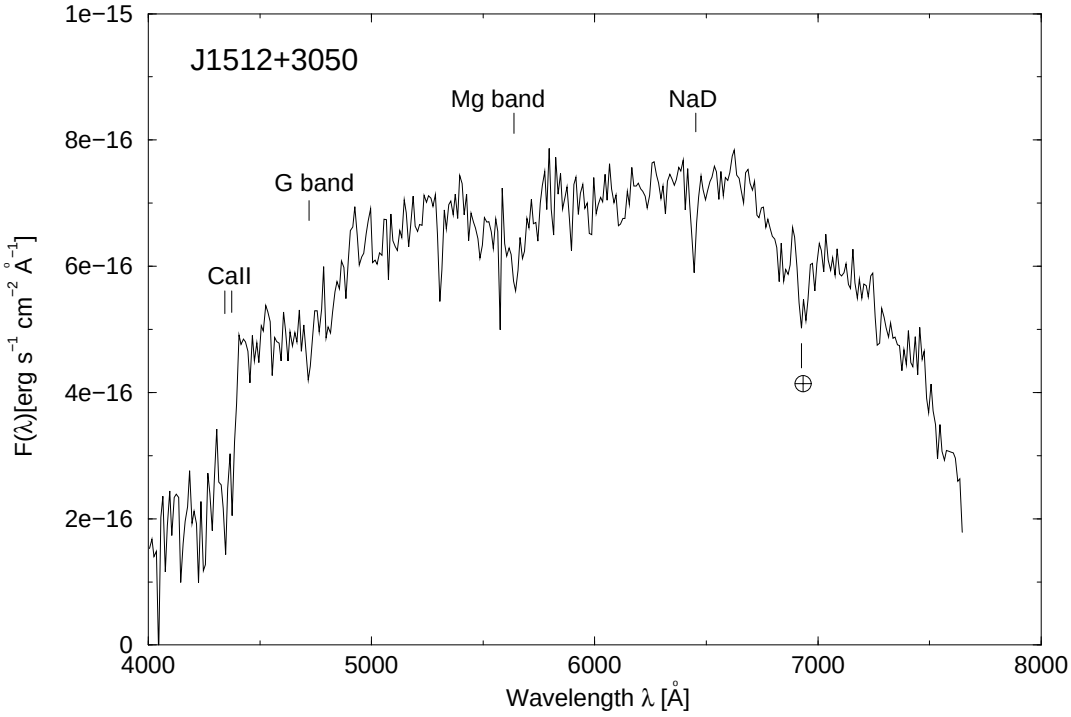

Fig. 4l. As in Fig. 4a but for the galaxy identified with the source J1512+3050

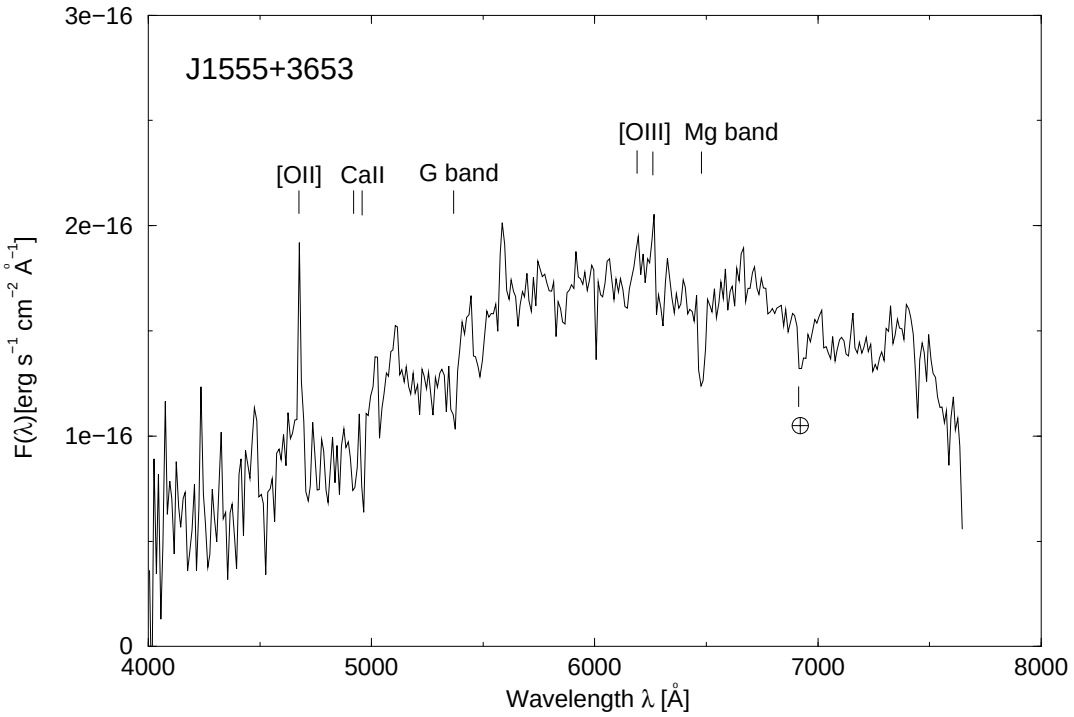

Fig. 4m. As in Fig. 4a but for the galaxy identified with the source J1555+3653

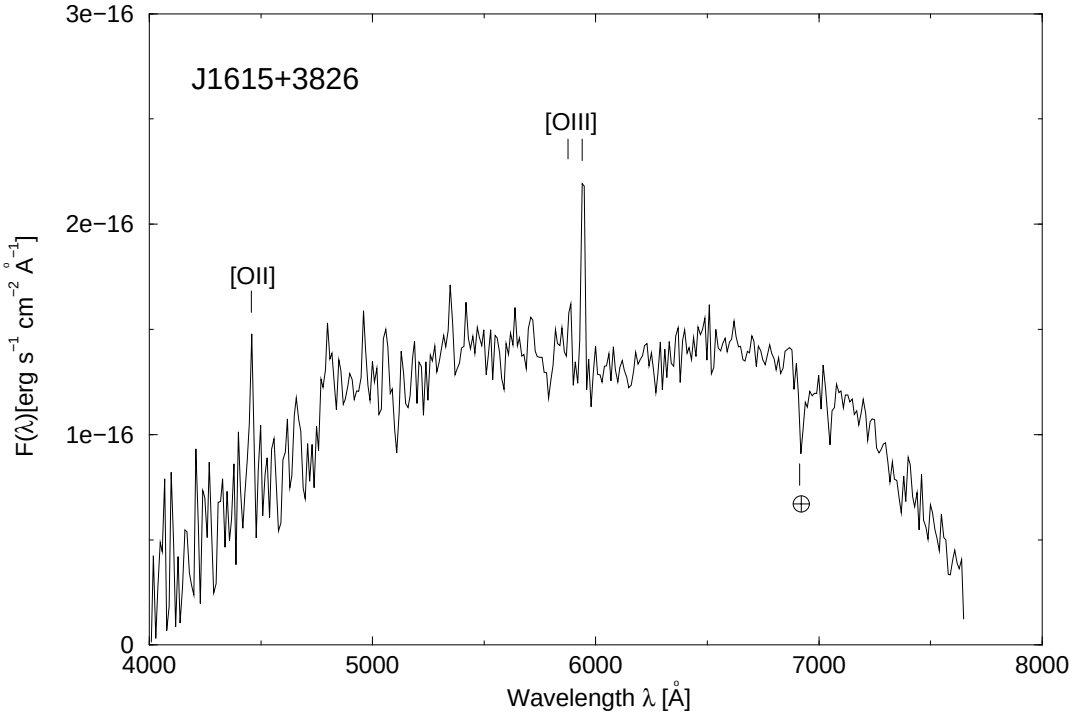

Fig. 4n. As in Fig. 4a but for the galaxy likely identified with the source J1615+3826

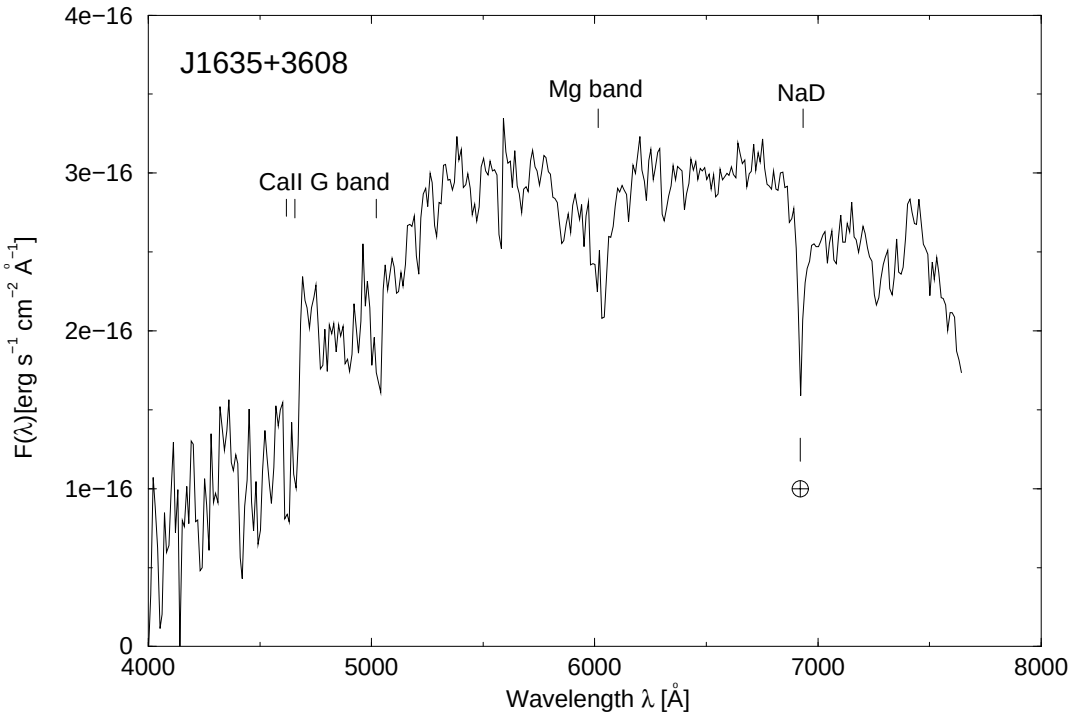

Fig. 4o. As in Fig. 4a but for the galaxy identified with the source J1635+3608